NTNU

Norwegian University of
Science and Technology

Optimization and Modeling of electrode structure and composition for novel PEM water electrolyser MEAs

Amin Hossein Zavieh

Light Metals Production
Submission date: June 2011
Supervisor: Frode Seland, IMTE

Norwegian University of Science and Technology
Department of Materials Science and Engineering

Acknowledgment

The present project was conducted at Norwegian university of technology in Trondheim as a part of the Master degree.

It is my privilege to express my sincerest regards to my project supervisor and co-supervisor, Dr. Frode Seland and Dr. Magnus Thomassen, for their valuable inputs, able guidance, encouragement, whole hearted cooperation and constructive criticism throughout the duration of the project.

I deeply express my sincere thanks to Dr. Edel Sheridan and Dr. Anders Ødegård, for all their inputs, patience during my training, inspirations and generous helps, without which finishing this project was impossible.

Last and certainly not least, I would like to thanks my parents for their love and support.

Summary

Lack of commercial electrocatalysts and membrane electrode assemblies (MEA) which are efficient, durable and reasonably priced for proton exchange membrane water electrolysis was the inspiration of the current project.

A reliable, reproducible and optimized membrane electrode assembly preparation protocol for water electrolysis was developed, with emphasis on the oxygen evolution electrode. The MEAs comprised of a Nafion® 115 membrane with commercially available 20 wt% Pt on carbon and in-house synthesized 20 wt% Ir on antimony tin-oxide, manually sprayed onto the membrane using an airbrush, and functioning as the hydrogen and oxygen evolution catalysts, respectively. A current density of 2.1 A/cm^2 was obtained at a cell voltage of 1.85 V and 80 °C.

In-situ electrochemical characterization such as steady state polarization and cyclic voltametry was performed on the MEAs to be able to predict performance in stationary applications. Effect of loading on cell performance at different cell voltages was studied and 0.8 mgIr/cm^2 loaded MEA showed the highest current at 1.85V. Furthermore, cross section and morphology of the catalyst was studied using SEM and TEM. The catalyst layer thickness found to be from 2 to 5 μm for 0.4 to 1.0 mgIr/cm^2 loadings.

A theoretical one-dimensional model was proposed for current and reaction rate distribution through the catalyst layer. Since the conductivity of the catalyst measured to be higher than Nafion, model shoed at high loadings and potentials (or catalyst layer thicknesses) reaction tends to happen mostly near the membrane while at low loadings and potentials reaction rate is uniform though the layer. In addition, model was compared to experimental data and shown it is reliable for low potentials but it needs some correction for high potential due decrease in specific active area per volume by reducing thickness of the layer and not taking other factors than Tafel polarization into consideration.

Introducing accelerated degradation protocol, durability of the catalyst was studied and corrected by subtracting ohmic losses due oxidation and etc. The loss for accelerated degradation found to be 0.3 mV/h. Then structure of the MEA cross-section was investigated using TEM after degradation test so major cause of the loss in performance found to be migration of Iridium nano particles into the membrane

Contents

Table of figures

Symbols

a	specific interfecial area per volume, 1/cm
α	asymmetry constant
E	potential, volt
F	faraday's constant coulomb/g-equivalent
G	gibbs free energy, joule
H	enthalpy, joule
I	over all current density in one dimentional porous electrode,amp/cm2
i_0	exchange current density,amp/cm2
i_1	current density in the matrix phase, amp/cm^2
i_2	current density in the pore electrolyte, amp/cm^2
j	i/I
L	thickness of the catalyst layer
n	nukber of electron in equation for electrode reaction
p	pressure, bar
R	gas constatnt joul/mol-deg
S	enthropy, joule/degree
T	temperature, degrees kelvin
t	time, second
x	distance through the one-dimentional porous electrode, cm
μ	Chemical potential, volts
θ	integration constatnt for Tofel polaroization
κ	conductivity of pore electrolyte S/cm
σ	conductivity of matrix S/cm
Φ_1	potential of matrix phase, volts
Φ_2	potential of pore electrolyte, volts
ψ	integration constatnt for Tofel polaroization

1 Introduction

As the energy demand increases, consumption of fossil fuels increases, which leads to an increasing release of greenhouse gases and growing environmental concern among the public. The fossil fuels are finite in amount and eventually within a few decades the availability will reach a peak where oil and gas become too expensive to be used as an energy carrier. Fossil fuels are unevenly distributed throughout the world and less access to this energy source may cause serious international conflicts. Additionally, as time goes by non-energy use will be the only economical application of fossil fuels [1].

Releasing CO_2 into the atmosphere and its impact on global warming has caused major concerns worldwide and has led to Kyoto agreements on the reduction of CO_2 emission. There are still many disagreements about the connection between CO_2 emission and global warming; however, there exist a general acceptance to carry on a "no regret policy" and to take necessary actions [2].

Hydrogen as an energy carrier, generated from renewable energy sources, constitutes an environmental friendly solution to the world energy problem in the future. After oil-crisis and public awareness of the pollution caused by combustion of fossil fuels, rapid development of clean energy systems has taken place during the last decade [3]. In particularly the development of fuel cell technology, where hydrogen together with oxygen is elctrochemically converted to electrical energy and water, has promoted the use of hydrogen as a fuel in vehicle propulsion. Today, fuel cell technology research has been committed by most of the largest car producers and research and development is in rapid progress.

An eco friendly ideal cycle to produce electricity and use hydrogen as an energy carrier is shown in figure 1-1. In this cycle, electricity from renewable energy sources is used to electrochemically split water into hydrogen and oxygen. The hydrogen may then be stored, before being electrochemically oxidized in a fuel cell to form electric power and water. The only input to this cycle is the clean renewable energy and the only output is electric power [3].

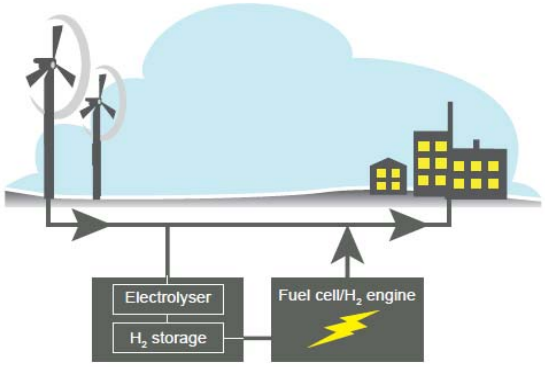

Figure1-1 Ideal energy cycle involving hydrogen

Since the introduction of polytetrafluorethylene (PTFE) and development of Nafion (Du Pont) in the 1960's, which showed rather high proton conductivity with a high water content. The Nafion membrane introduced a new kind of fuel cells, and paved the way for rapid development of the PEM fuel cell. A PEM water electrolyser building on the same technology as the PEMFC, has attracted some attention over the last few decades [4-7]. PEM electrolysis have certain advantages over the conventional alkaline water electrolysers that are dominating the market today. Due to the lack of a circulating liquid in PEM systems, small mass and overall dimensions, low power consumption, high current densities, low parasitic energy losses, rapid start-up/shut-down rates and production of very high purity gases are made possible [4]. Obvious disadvantage of the PEM system is the poor oxygen evolution kinetics and expensive catalyst materials due to the acid environment. Development of the electrode catalysts, and then in particular the electrocatalyst for oxygen evolution (anode catalyst) is of great importance to improve the total efficiency of the PEM electrolyser [3, 8].

1.1 Hydrogen Production

Hydrogen can be produced in many ways, for example via the processing of hydrocarbons (e.g. steam reforming), by water electrolysis (table 1-1), photochemical reactions, or by biological processes. When water electrolysis is carried out using renewable energy (e.g. Hydro, Wind, and Solar) the hydrogen can be considered as a completely renewable and clean energy carrier. It is important to remember that hydrogen is only the energy carrier and therefore electrochemically produced hydrogen is only as clean as the primary energy source.

Table 1-1: Major methods of hydrogen production through water electrolysis

Alkaline electrolysis
Proton exchange membrane (PEM) water electrolysis
Steam electrolysis
Hydrogen as a byproduct from Chlor-alkali production or electrowinning of metals in aqueous solutions

Water electrolysis offers several advantages over other production methods such as steam reforming such as no carbon emissions, very pure hydrogen that avoids CO poisoning in fuel cells, no dependence on hydrocarbon sources simplicity in small scale/ real time supply, utilization of renewable primary energy sources and pure oxygen as a by-product [3]. There are of course some challenges as well regarding to water electrolysis for instance it needs hydrogen storage for fluctuating primary energy supply and inexpensive renewable energy sources.

PEM systems offer several advantages compared to the traditional alkali based systems (table 1-4) [8].

Table 1-4: Advantages of PEM electrolysis for hydrogen production

Higher performance / efficiency
Much higher current densities (up to 13 A cm^{-2} reported [10])
Wide range of current densities = flexible production rate
Very pure H2 and O2
Greater safety (no circulating caustic electrolyte)
High differential pressure across membrane is possible
Inherent gas separation by membrane electrolyte
Possibility of combined fuel cell / electrolyser

1.2 Present Work

The present project was conducted at the department of Materials Science and Engineering at Norwegian university of technology in Trondheim as a part of the Master degree. This project is a part of an EU-project called NEXPEL and it was done in collaboration with the researchers at Sintef materials and chemistry in Trondheim.

There are two essential motivations behind this project work, first is the above mentioned advantages of PEM electrolyzers and the second is the lack of commercial electrocatalysts and

membrane electrode assemblies (MEA) which are suitable, efficient, durable and of course reasonably priced for the purpose. This master's thesis work is founded on the findings of Egil Rasten, [8], who ultimately chose Iridium as the base electrocatalyst material for oxygen evolution, and developed a spraying technique for the preparation of MEA, in accordance to the patent by R.D. Mussel et al. [11]. The main objectives of this project have been to:

- Create a reliable and optimized MEA preparation protocol
- Characterize the synthesized catalyst in an operating PEM water electrolyser unit
- Optimize and study the effect of oxygen evolution catalyst loading on the performance of a cell
- Develop a theoretical model for the porous catalytic layer
- Compare the theoretical analysis to experimental data, and study the causes of deviation

2 Theory

The basic principle for any water electrolysis system can be easily described as electrochemical splitting of water molecules to hydrogen and oxygen. Without any elaboration, at proton exchange membrane (PEM) water electrolysis cells, running water through anode, decomposes to protons, electrons and oxygen, then protons are transported through the proton conductive membrane to the cathode at which they combine with the electrons coming from the outer circuit driven by the potential supply and form hydrogen gas. The schematic view of the PEM water electrolyser is shown in figure 2-1.

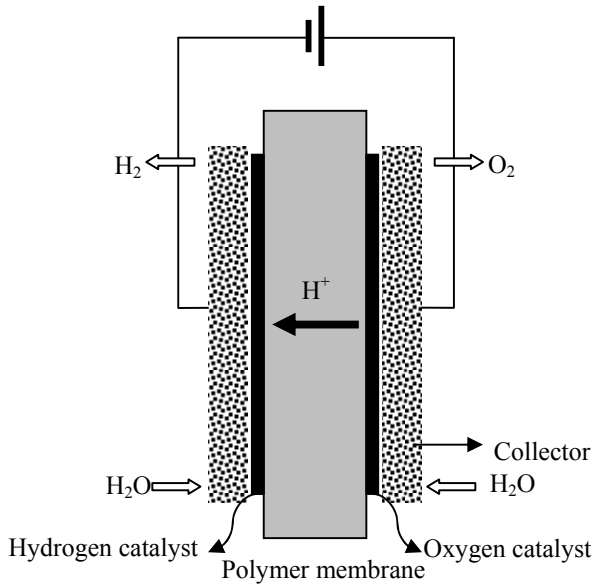

Figure 2-1 schematic view of PEM water electrolyzer

In this case the cathodic, anodic and net reaction are shown in equation

Cathodic : $2H^+ + 2e^- \rightarrow H_2$ (2-1)

Anodic : $H_2O \rightarrow ½\ O_2 + 2H^+ + 2e^-$ (2-2)

Net Reaction : $H_2O \rightarrow ½\ O_2 + H_2$ (2-3)

2.1 Thermodynamics and kinetics

The minimum potential difference which must be applied between two electrodes of an electrolyser is thermodynamically defined in terms of Gibbs free energy change of reaction 2-3

$$E = -\frac{\Delta G}{nF} \qquad (2\text{-}4)$$

Where $\Delta G = \mu_{H2} + ½\ \mu_{O2} - \mu_{H2O}$ (2-5)

μ is chemical potential and ΔG is a positive quantity for reaction 2-3 as written. From equations 2-4 and 2-5 (Nerst equation):

$$E^{rev} = -\frac{\Delta G^{\circ}}{nF} - \frac{RT}{2F}\ln\left(\frac{P_{H_2}P_{O_2}}{a_{H2O}}\right) \qquad (2\text{-}6)$$

Where n is the number of electrons involved, F is Faraday's number, P is partial pressure and a is activity.

E^{rev} measures the difference between the reversible potentials of the anode and the cathode (equilibrium cell voltage) which is the lowest potential that must be applied for the reaction to happen. Under standard conditions at 25°C and water in liquid form, $\Delta G° = 237.178$ kJ/mol^{-1} [12] the E^{rev} is calculated to be 1.229 V. Equation 2-6 shows that E^{rev} is increased by an increase in partial pressure. Moreover, E^{rev} is decreased by increasing temperature therefore thermodynamics suggests that the best conditions for operating in case of saving energy would be met at high temperatures and low pressures if water remains in liquid state since at very high temperature (steam water electrolysis) the benefit of E^{rev} is quite clear.

The energy balance for the cell can be written, in which ΔH is the measure to break and form bonds between molecules. Equation 2-7:

$$\Delta G = \Delta H - T\Delta S \qquad (2\text{-}7)$$

This leads to the standard state equation for thermoneuteral conditions given by the following equation:

$$U_{tn} = -\Delta H/nF \qquad (2\text{-}8)$$

When the cell potential U_{cell} equals to the thermoneuteral potential (U_{tn}) there is no heat exchange between the cell and surroundings, for less potential cell absorbs heat and for higher amount cell produces heat. At standard condition and water in liquid form U_{tn}= 1.48 V. For the overall reaction the thermal efficiency can be written as

$$\varepsilon_t = U_{tn} / U_{cell} \qquad (2\text{-}9)$$

Whereas the energy efficiency in terms of Gibbs energy can be defined as

$$\varepsilon_{\Delta G} = E^{rev} / U_{cell} \qquad (2\text{-}10)$$

There are other factors than thermodynamics which affect current vs. potential, including electron transfer, transport and chemical processes. Therefore kinetics of the reaction and slowest reaction step which can be an electron transfer or diffusion should be taken into consideration.

The magnitude of this deviation from what thermodynamics predict at anode or cathode, is termed overpotential, defined as

$$\eta = E - E^{rev} \qquad (2\text{-}11)$$

At low current densities the rate of change of electrode potential is controlled by transfer of electrons across the boundary layer between electrode and the solution which is called electron transfer or activation overpotential. At higher current densities the electron transfer is no longer the limiting step, and the limitations are because of slow diffusion of reactants from the solution to the boundary layer to react, which is called mass transport overpotential. On the other hand if a chemical reaction coupled with the electron transfer reaction was struggle to keep up with the other steps and makes a limitation it is called reaction overpotential. Furthermore, resistance towards movement of ions in the electrolyte and electrons in the electrodes and connecting wires leads to another voltage loss, commonly referred to as the ohmic loss, *IR*. The total cell voltage that is required in order to produce hydrogen and oxygen at a certain rate (current) comprises of the thermodynamic voltage and the various loss terms according to [13]:

$$U_{cell} = E^{rev} + \eta_{anodic} - \eta_{cathodic} + IR \qquad (2\text{-}12)$$

In a nutshell, to decrease the potential of cell in order to reduce energy consumption we have to decrease each terms of equation above which can be called losses of our system. For instance, increasing the surface area or using more active catalysts increases kinetics of reaction hence decreases overpotentials. Resistance of the cell (membrane, backing plates, wires, bipolar plates and etc.) is of importance and by decreasing it term IR decreases so the cell potential reduces.

2.1.1 Understanding the origin of the current-potential (polarization) curve in the electron-transfer region

Assuming a simple charge transfer process:

$$Ox + ne^- \leftrightarrow Red \qquad (2\text{-}13)$$

The forward is cathodic and reverse is anodic reaction; Ox and Red stand for oxidized and reduced species. The net current density for the reaction will be the sum of both anodic and cathodic current densities and known as Butler-Volmer equation:

$$j = j^{+} + j^{-} = j_0[\exp(\frac{(1-\alpha)nF\eta}{RT}) - \exp(\frac{(-\alpha)nF\eta}{RT}) \qquad (2\text{-}14)$$

Where j is current density (cd), j_0 is the exchange current density, α is asymmetry parameter, η is the overpotential and E is the applied potential. R, T and F has its usual meanings and n is number of electrons involved in the reaction. At high overpotentials, equation 2-14 can be solved for either anodic or cathodic direction, or lead to the well known Tafel equation:

$$\eta_{anodic} = b_{anodic}\, log\, (i/i_0) \qquad (2\text{-}15)$$

$$\eta_{cathodic} = b_{cathodic}\, log\, (i/i_0) \qquad (2\text{-}16)$$

Where b is the Tafel slopee given by:

$$b_{anodic} = \frac{-RTln10}{(1-\alpha)nF} \qquad (2\text{-}17)$$

$$b_{cathodic} = \frac{-RTln10}{\alpha nF} \qquad (2\text{-}18)$$

In equation 2-14, 2-17 and 2-18 α stands for asymmetry parameter which is usually close to 0.5 and express the activation barrier dependance of the electrochemical reaction [8].

Exchange current density j_0, depends clearly on the concentration of the species participation in the electrochemical reaction and free energy of activation. Its magnitude is an essential quantity in electrochemistry and in particular, it is the value of j_0 that is increased when electrochemical reaction is catalysed. A typical polarization curve is shown in figure 2-2 for water electrolysis cell consisting of E^{rev}, η_{anodic}, $\eta_{cathodic}$ and IR it can be seen that at high currents the curve is linear, which indicate that the IR loss term dominates the current-potential behavior in this current domain. Activation overpotential is most dominant at low current densities, and quickly diminishes in importance as the current density increases due to the exponential dependence on the potential.

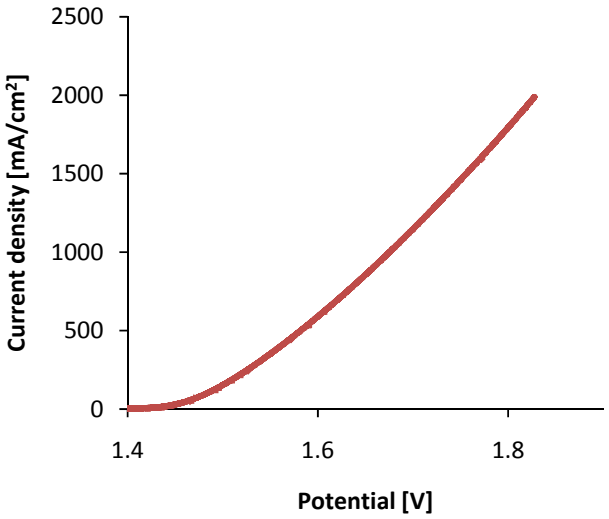

Figure 2-2 A typical polarization curve for water electrolysis cell

2.2 Electrode reactions and reaction mechanisms in PEM cells

2.2.1 Hydrogen evolution reaction

Among metals with intermediate bond-strength Platinum is known as the most active catalyst which is used both in Fuel cells and electrolysers, therefore a large number of Pt catalyst are available in commercial market, and companies try to increase the surface area thus decrease the necessary loading and reduce the cost [8].

Thermodynamically electrocatalytic oxides seem to be unstable to the potentials of hydrogen evolution, however they in fact evolve H_2 at low overpotential and exhibiting notable stability [14]. The electrochemical activity of the hydrogen evolution reaction (HER) on different metals can be compared using the energy of the chemisorbed H to the active sites. For the metals with high bond-strength the H desorption becomes the rate determining step and makes a barrier against the HER, for those with low bond-strength adsorption of the protons to the active sites becomes the limiting step and decrease the rate of the reaction, whereas metals with intermediate bond-strength show the highest activity toward the reaction [15] the above approach is shown in a so called Volcano plot figure 2-3:

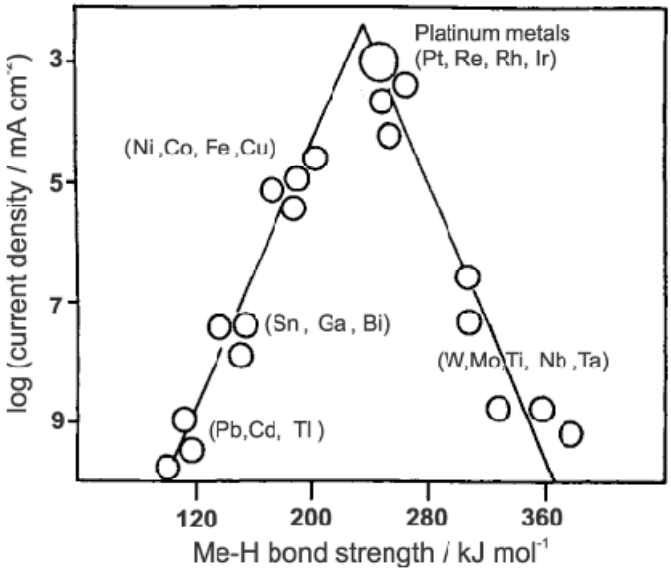

Figure 2-3 Volcano plot of the HER on different Metals [16]

Hydrogen evolution takes place at the whole active surface [17] which can be clarified by the fact that reacting particles do not need to travel from the bulk solution because H_2 evolution originates from water molecules and protons which are small enough to be found in cracks, pores, crevices and so forth and the supply can be practically assumed to be infinite.

HER also changes the voltametry response of an oxide. In case of Iridium and ruthenium oxide the shape of the cyclic voltametry is maintained where as the value of the charge as a rule increases [18]. This is attributed to two mechanisms first is erosion of the crystal face which result in higher surface roughness and increase in active sites and the second is wetting of less reachable surface regions promoted by H^+ discharge on oxide sites.

2.2.2 Oxygen evolution reaction

Oxygen evolution is a natural reaction on oxide surfaces, because these already contain the intermediates of the electrode reaction, and oxides are anyway formed anodically on metal electrodes as precursors of O_2 gas formation. Oxygen evolution is a demanding reaction so it is highly affected by nature and structure of the electrocatalysts [14]. In addition O_2 evolution combines the demand for activity with the demand for stability, because it takes place under severe electrochemical conditions [19].

There are many mechanisms proposed for oxygen evolution. Since all metals are covered by a thin oxide layer at potentials for oxygen evolution, mechanisms on oxide electrodes should be

taken into consideration. Oxygen evolution reaction involves formation and breakage of the bond between oxygen and oxide surface which shows that there are some material transformations involved as well as electrochemical processes. These complex processes lead us again to the volcano plot (figure 2-4) which is electrocatalytic activity versus enthalpy of the formation a higher or lower oxidation state [3].

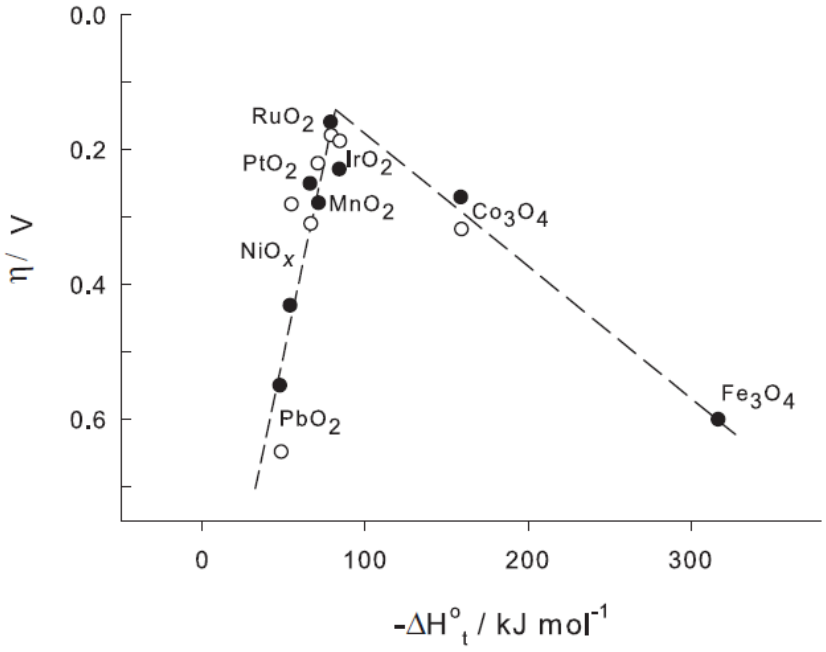

Figure 2-4 volcano plot, electrocatalytic activity of different oxide for OER vs. enthalpy of transformation from one oxidation state to another [20]

2.3 Proton exchange membrane water electrolysis cell

A proton exchange membrane (PEM) water electrolysis cell consists of a proton conductive solid membrane to which hydrogen and oxygen evolution catalysts are bonded, this whole body is called membrane electrode assembly (MEA). Figure 2-5 shows a complete PEMWE cell, which consist of MEA in the middle, flowfields on both side and pores plates which allow gas to evolve, the cathode side can be made out of graphite but the anode side should be a material which is stable at the oxygen evolution condition as well as being porous.

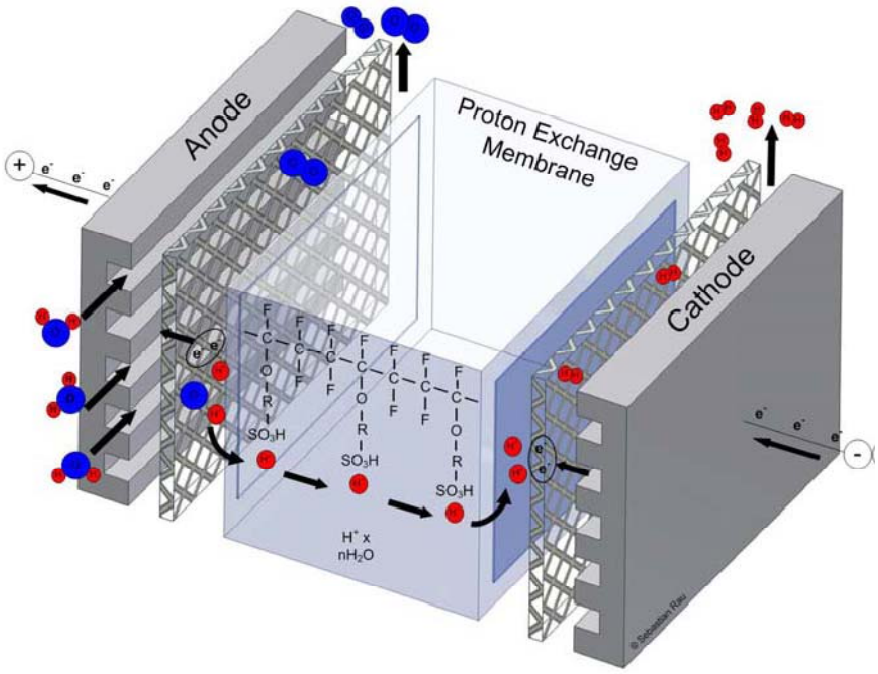

Figure 2-5 schematic of a single PEMWE cell

A complete electrolyser also needs a power system, water supply tanks and pumps for circulation and heating system both for water tanks and the cell

2.3.1 Bipolar Plates

The bipolar plates, which separate both electrodes of neighboring cells in multicell design (one anode of a cell and one cathode of the other), have three distinct roles [21]:

- To ensure the electron conductivity between two neighboring cells;
- To allow the distribution of reactants and provide water to active sites while
- Thermal management inside the elementary cell by evacuating the excess heat.

The bipolar plates are usually fabricated with non-porous machined graphite or corrosion-resistant metal plates. Porous metallic foams are commonly used for distributing the reactants. One key point is to ensure a low ohmic resistance inside the bipolar plate and at the contact with the MEA. Another point is to use materials with high corrosion resistance in the oxidative environment of the oxygen anode.

The flow of the water can be controlled by different patterns on the bipolar plates. The supposed problem of some designs is that bubbles may form and trap in some channels, leaving some areas of the electrode unsupplied with water and reducing the overall active area.

The material must also be able to be manufactured within the following requirements [22]:

- The bipolar plate must be slim, for minimum stack volume.
- It must be light, for minimum stack weight.
- The production cycle time should be reasonably short.

As a component in PEMWE, metal bipolar plates should have very high corrosion resistance because any metal ions generated from the corrosion process can migrate to the membrane, lower the ionic conductivity of the membrane, and thereby degrade the performance of the stack. Moreover, any corrosion layer will lower the electrical conductivity of the bipolar plates and thus increasing the cell voltage of the PEMWE unit due to the high electrical resistance [23].

2.3.2 Solid polymer electrolyte membrane

Among different produced solid polymer membranes, the most well known and well established one is sulphonated fluoropolymers known as Nafion (DuPont).

For the production of the membranes the first step is to use polyethylene which is based on ethylene. In the mentioned polymer hydrogen molecules are substituted by fluorine in a so called process perfluorination and the monomer is called tetrafluoroethylene. The modified polymer shown as backbone in figure 2-6 is called polytetraflourethylene and also known as PTFE. It is a hydrophobic polymer and branded as Teflon, that has had a significant role in development of fuel cells [24]. Durability and resistance to chemical attack are also important properties of this polymer which are the result of the strong bonds between carbon and fluorine.

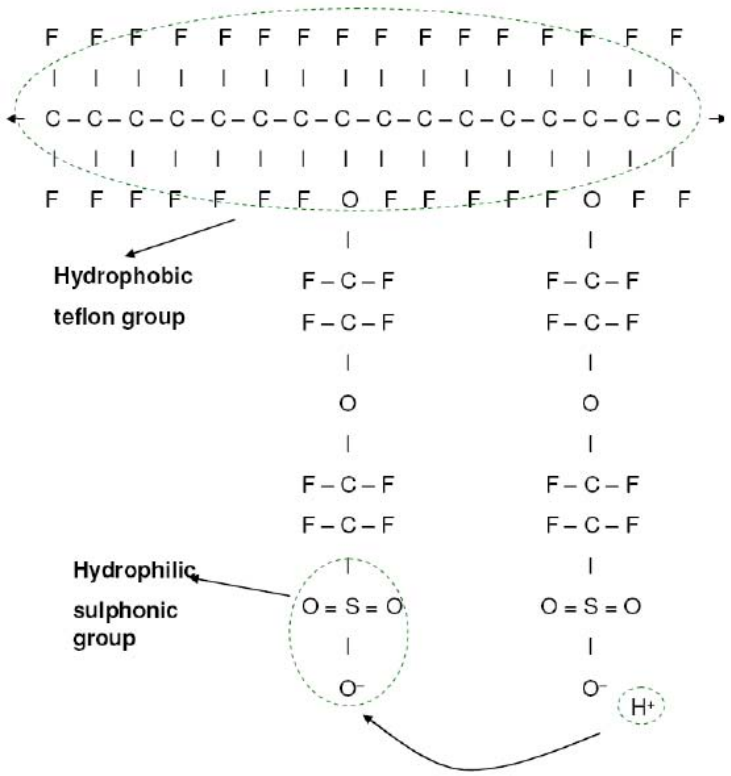

Figure 2-6 Chemical structure of Nafion [22]

Last step to produce a proper membrane is adding a side chain, ending with sulphonic acid HSO_3. The complete polymer is shown in figure 2-6. The side chain is highly hydrophilic due to the properties of sulphonic acid and presence of SO_3^- and H^+ ions cause a strong mutual attraction between molecules giving the chains a tendency of forming clusters within the overall structure of the material [22]. The structure of Nafion membrane materials with long chain molecules containg hydrated regions around the sulphonated side chains are shown in figure 2-6, exhibits the hydrophilic regions around the clusters of sulphonated side chains lead to the absorption of large quantities of water. Water facilitates proton transport within the Nafion membrane and lead to rather high proton conductivity [25].

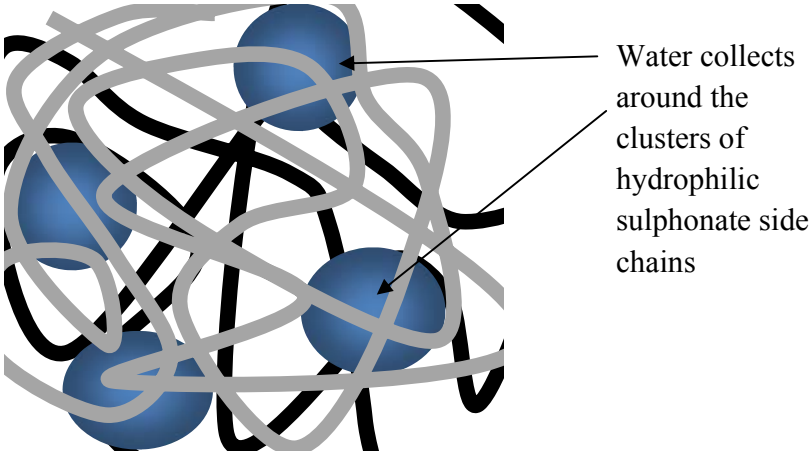

Figure 2-7 The structure of Nafion-type membrane materials

The main features of Nafion and other fluorosulphonate ionomers are [22]:

- Chemically highly resistant
- Mechanically strong and can be made into very thin films
- Acidic
- Large quantity of water absorption
- Highly proton conductive

Nafion membranes are used with different thicknesses; the lower the thickness is, the higher the conductivity and the lower ohmic drop of the cell but on the other hand decreasing the thickness results in the higher permeation of the gas. Therefore an optimum thickness should be found according to the cell design and the usage [25]. The effect of thickness on resistance is shown in figure 2-8.

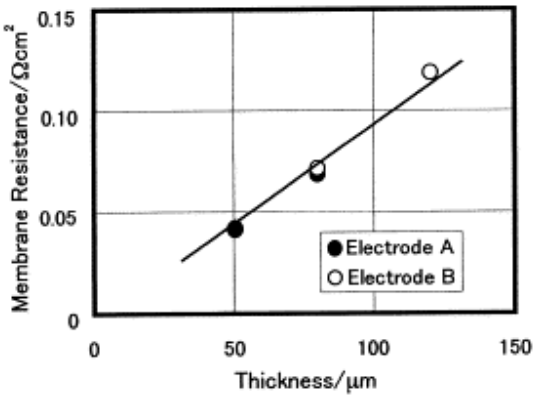

Figure 2-8 Dependence of membrane resistance on membrane thickness. Current density: 0.5 mA/cm2 [25]

Boyer et al. [26] measured the proton conductivity in the active layer of PEM gas diffusion electrodes, they suggested a model for the effective conductivity in an electrode with a mixed conductive phase. Figure 2-9 shows the specific conductivity versus volume fraction of Nafion in the layer.

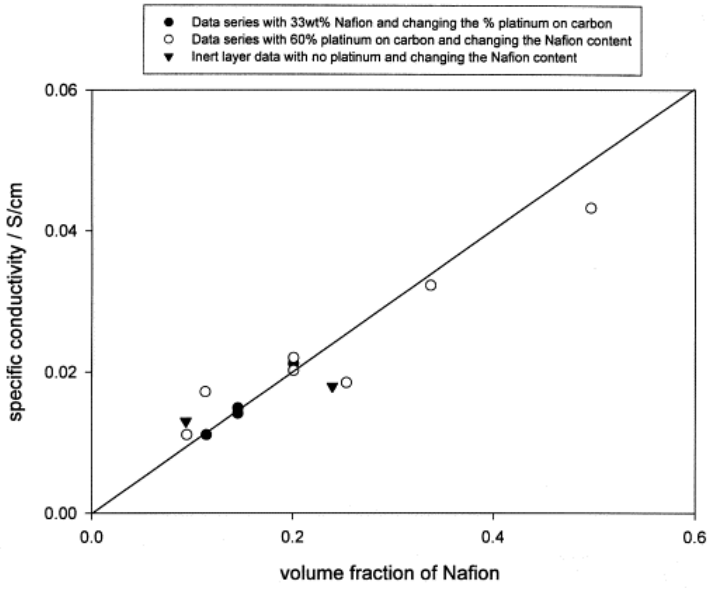

Figure 2-9 Plot showing the effective specific conductivity vs the volume fraction of Nafion in the composite layer for each series of experiments. The line shows the fit using the bulk conductivity value [26]

2.3.3 Electrocatalysts

Although thermodynamical potential of water splitting is 1.23 V, slow kinetics and other losses leads to high overpotentials in the cell, to improve reaction kinetics, active electrocatalysts with high surface area are used on both hydrogen and oxygen evolution electrodes. Nobel metal oxides are well known electrocatalysts in industrial processes and many individual oxides and composition of oxides has been studied for the purpose, for instance in Trassati's work [14] 35 different oxide compositions are listed which has been characterized towards the oxygen evolution.

Based on A. Marshall's PhD study [3] IrO_2 and RuO_2 are the best electrocatalysts to be used for OER. RuO_2 shows the highest activity but it shows low stability at the operating condition, so it should be stabilized by another oxide such as IrO_2 or SnO_2.

There are several factors that are required for an excellent electrocatalyst [4]:

- High surface area
- High electrical conduction
- Good electrocatalytic properties
- Long-term Mechanical and chemical stability
- Minimized gas bubble problems
- Availability and lost cost
- Health and environmental issues

Active surface area and particles structure highly manipulate the activity and performance of the electrocatalysts. Since noble metals are expensive, in order to utilize PEM water electrolyzers activity and active surface area should be increased while amount of Nobel metal used is decreased. To gain this, supports for the electrocatalysts are used, the support materials are necessary to obtain a high dispersion and a narrow distribution of oxides nanoparticles, which is the prerequisite to obtain a high catalytic performance of catalysts. The support materials can also interplay with catalytic metals, which influence the catalytic activity. The durability of the catalyst is also greatly dependent on its support. Generally, the requirements for catalyst support materials can be summarized as [27]: 1) high specific surface area, which is necessary for improving the dispersion of catalytic metals, 2) high electrochemical stability under water electrolysis operating conditions, 3) high conductivity, and 4) easy-to-recover oxides in the used catalyst. In addition, the interaction between catalytic metals and the support materials should be considered in improving the catalytic activity and durability.

Different catalyst structures are predicted. Figure 2-10 shows various catalyst structures, 2-10a shows dispersed homogenous catalyst, 2-10b shows agglomeration of the catalyst which should be porous to have high surface area and necessary active sites, 2-10c is a support particle with the nano sized catalyst particles attached to its surface and 2-10d shows a support with a thin shell of the active catalyst. Structures shown in 2-10c and 2-10d can drastically increase the utilization of the catalyst by decreasing the loading of the noble metal and cost of the cell as well as catalytic activity due to synergetic effect [3].

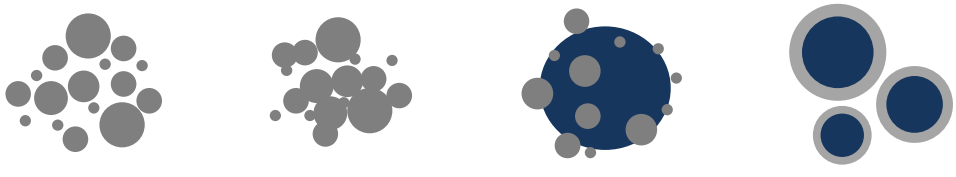

Figure 2-10 Different catalyst structures : a) monodispersed catalyst with homogenous composition b) agglomeration of the catalyst c) classic structure with a small particles attached to a support d) core-shell structure with a support in the core and catalyst on the shell

2.4 Cell and catalyst ink characteristics

Prior to this research, a master project was done in fall 2010 [28] by the same author on optimizing different variables in cell and ink such as temperature, clamping pressure, Nafion content and water to iso-propanol ratio in the ink.

Cell temperature and clamping pressure was chosen to be 80°C and 6 bars respectively due to improved kinetics and improved electronic conductivity between the catalyst layer and collector plates. Figure 2-11 shows effect of temperature and clamping pressure on weight normalized current at 1.8 V.

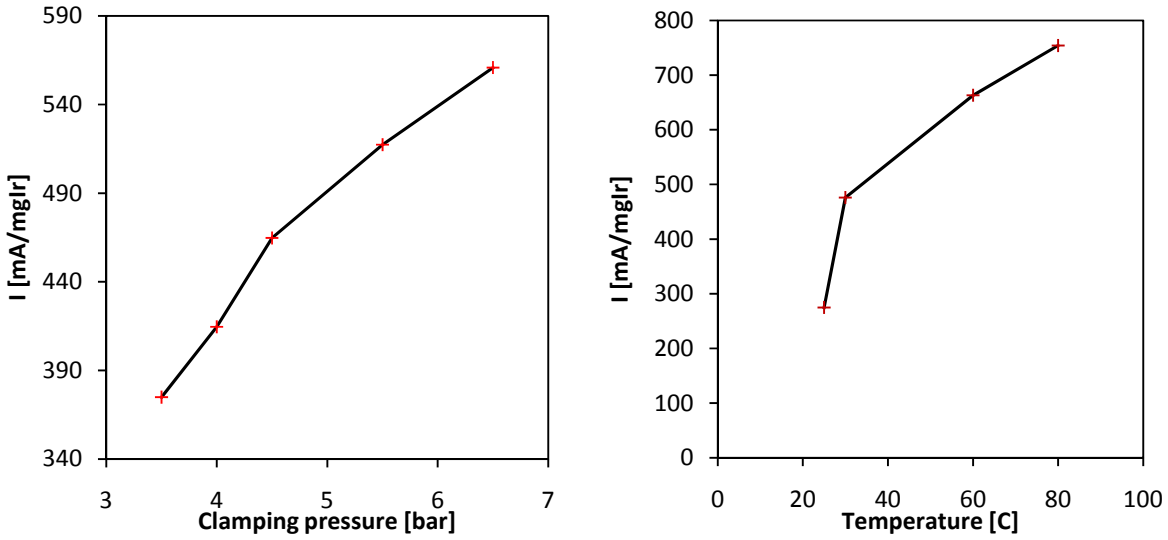

Figure 2-11 effect of a) clamping pressure and b) temperature on normalized current at 1.8V [28]

Figure 2-12 shows the effect of different Nafion contents on weight normalized current at 1.8 V where 7.5 wt% Nafion refers to the highest performance. Too low content of Nafion in catalyst layer can reduce the three-phase interface and decrease the adhesion between the catalyst layer and the Nafion membrane, result in lower current densities at the same potentials. The low bonding and adhesive force will also lead to easy breaking and washing away of the layer due to the water flow. On the other hand too much Nafion content can result in high resistivity and covering the catalyst in the way that avoids electron exchange.

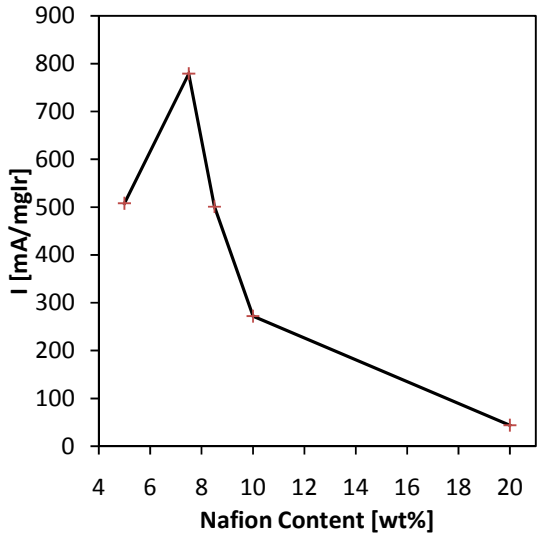

Figure 2-12 effect of Nafion content on normalized current at 1.8V [28]

2.5 Porous Electrodes

Porous electrodes have many industrial applications mainly because they increase the contact area of the electrode material with solution or a gashouses phase. Generally their advantages can be summarized in [29]:

1. Rate of heterogeneous electrochemical reactions can be slow. A porous electrode can compensate for this by providing a large interfacial area per volume.
2. Double-layer adsorption constitutes the basis for novel separation processes involving cycling of the electrode potential. Just as in conventional fluid solid adsorption, a high specific interfacial area is desirable.
3. Important reactants may be stored in the solution in close proximity to the electrode surface. This permits sustained high-rate discharge for example in a lead-acid cell.
4. A diluted contaminant can be removed effectively with a flow-through porous electrode.
5. Nonconducting reactants of low solubility can also be stored close to the electrode surface.
6. The compactness of porous electrodes can reduce the ohmic potential drop by reducing the distance through which current must flow. This has obvious advantages in reducing losses in batteries and fuel cells.

Porous catalytic layers in a proton exchange membrane electrolyser are made of small agglomerates. In this study these agglomerates contain ATO (Antimony Tin Oxide) supported Iridium particles. They are bonded together and to the membrane by Nafion. Nafion not only

plays the role of a binder for the catalyst particles but also provides ionic conduction pathways between Iridium and the bulk membrane.

This porous three phase interface allows effective 1) gas and water diffusion, 2) proton transport and 3) electron transport to and from catalytic sites. A lot of studies have been directed towards optimizing the ratios of catalyst, support, Nafion and more importantly on the active surface area present in this three phase interface [30]. The performance of a PEMWE depends mainly on the surface area of the Iridium catalyst particles supported on the ATO. Many studies have been focused on determination of how the electrocatalyst particle size and catalyst loading on support affect specific activity and performance [31, 32]. However the effect of the amount of catalyst per area of the PEMWE MEAs has not been given the attention it requires.

Proper understanding of the microscopic structure of the catalyst layer is required to study the effect of any variable in this region. The catalyst layer can be described as a mixture made of catalyst particles (in our case, Ir on ATO), which are covered by the polymer ionomer membrane (usually Nafion). A schematic illustration (figure 2-13) based on a high resolution transmission electron microscope (TEM) image of the catalyst is proposed here to describe the cathode catalyst layer and reaction. Figure 2-13 shows that the active catalyst layer region contains small agglomerates consisting of ATO, Iridium and proton ionomer, separated by gas pores. Of course, the ATO particles are, in fact, not spherical but have a variety of complex and fractal type shapes. The protons are transported by diffusion and convection through the polymer phase of the agglomerates. Water arriving from the backing layer diffuses through the gas pores and the ionomer surrounding the catalyst particle.

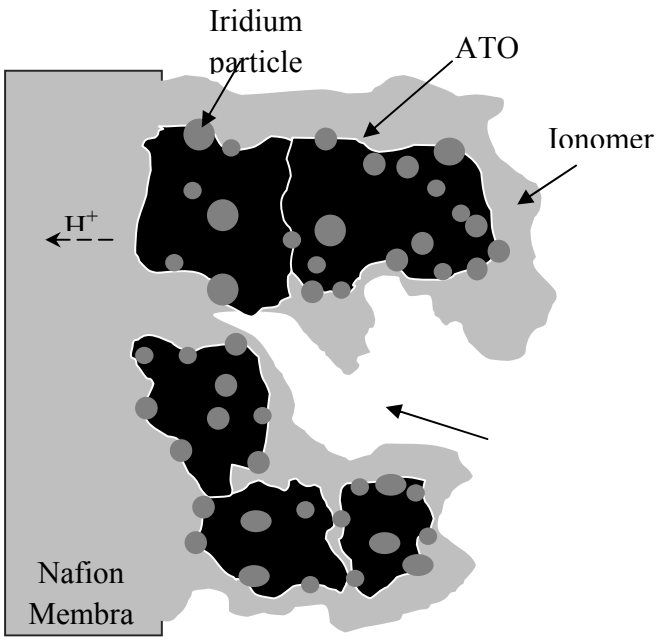

Figure 2-13 schematic illustration of the catalytic layer on the oxygen side

2.5.1 Theoretical Analysis of Current Distribution in porous electrode

Theoretical analysis of current in such a complex system requires a model include basic features and characteristics of an actual electrode, without going in to exact geometric details. In addition, the model should be described by parameters which can be obtained by suitably simple physical measurements such as volume-average conductivity, porosity and average surface area per volume. An appropriate model would involve different measurable averages over a region (depends on the model this region can have one to three dimensions) that is small with respect to overall dimensions and large compared to pore size. The model proposed in this section is based on Newman and Tobias' theoretical modeling of porous electrodes [33].

In this case a porous electrode flooded with electrolyte and backed by a solid metallic conductor of negligible resistivity (gold). Figure 2-14 shows an assumed one dimensional porous layer and the equation was solved for a one-dimensional field, uniform concentration, and Tafel polarization was assumed. By one-dimensional we mean that quantities such as potential, current densities and concentrations only vary with depth within the electrode. These assumptions are worthwhile since yields results showing the general behavior of porous electrodes and it is practically applicable.

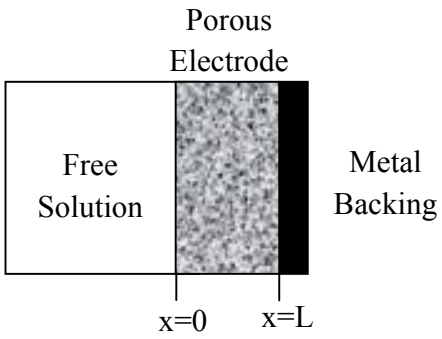

Figure 2-14 schematic of a on dimensional porous electrode layer

We shall also assume the shape characteristics and volume percentage of pores are uniform throughout the thickness of the electrode and the fluid velocity is zero in the electrode. Furthermore, calculations are in steady state mode in such way that time does not appear in an explicit manner.

Considering the condition at which the concentration is uniform, we apply ohm's law:

$$i_2 = -\kappa \frac{d\Phi_2}{dx}, \quad i_1 = -\sigma \frac{d\Phi_1}{dx}, \quad \frac{di_1}{dx} + \frac{di_2}{dx} = 0 \text{ (2-19, 2-20, 2-21)}$$

Where

i_1= current density in the matrix phase, amp/cm^2
i_2= current density in the pore electrolyte, amp/cm^2
Φ_1= potential of matrix phase, volts
Φ_2= potential of pore electrolyte, volts
κ = conductivity of pore electrolyte S/cm
σ = conductivity of matrix S/cm

and conductivities are constant. Since concentrations have been assumed uniform, the polarization equation is essentially independent of concentration. The following boundary conditions are suggested.

At $x = 0$, $i_2 = I$, $i_1 = 0$, $\Phi_2 = 0$.

At $x = L$, $i_2 = 0$.

These boundary conditions implies that at the metal backing, the current is carried entirely by the matrix while at the electrode solution interface the current is carries entirely by the pro electrolyte. Somewhere inside the electrode, between $x = 0$ and $x = L$ the current is transferred from the solution to the matrix, and local reaction rate is proportional to di_1 /dx.

To solve this problem analytically, linear or exponential current potential relation is applicable. For Tafel polarization in the anodic case

$$\frac{di_2}{dx} = ai_0 \exp\{\beta(\Phi_1 - \Phi_2)\} \qquad (2\text{-}22)$$

Where

$$\beta = (1-\alpha)\frac{nF}{RT} \qquad (2\text{-}23)$$

The cathodic case can be solved in a completely analogous fashion. By integration equation 2-21 and differentiation equation 2-22 and eliminating Φ_2, Φ_1 and i_2 one obtains

$$\frac{d^2 i_1}{dx^2} = \frac{di_1}{dx}\beta\left\{\frac{I}{\kappa} - i_1\left(\frac{1}{\kappa}+\frac{1}{\sigma}\right)\right\} \qquad (2\text{-}24)$$

By introducing quantities

$$y = \frac{x}{L}, \quad j = \frac{i_1}{I}, \quad \delta = L|I|\beta\left(\frac{1}{\kappa}+\frac{1}{\sigma}\right), \quad \text{and} \quad \varepsilon = \frac{L|I|\beta}{\kappa}$$

A dimensionless, nonlinear differential equation for the current is finally obtained

$$\frac{d^2j}{dy^2} = \frac{dj}{dy}(\delta j - \varepsilon) \qquad (2\text{-}25)$$

With the boundary conditions

$j = 0$ at $y = 0$ and $j = 1$ at $y = 1$

The latter can be reduced to a first-order equation because variable y does not appear in this equation using

$p = \frac{dj}{dy}$, so that $\frac{d^2j}{dy^2} = p\frac{dp}{dj}$ then the first integration is straight forward, and the second integration, somewhat more involved, may be found in standard mathematical tables. The solution is

$$j = \frac{\tan(\theta y - \psi) + \tan(\psi)}{\tan(\theta - \psi) + \tan(\psi)} = \frac{2\theta}{\delta}\tan(\theta y - \psi) + \frac{\varepsilon}{\delta} \qquad (2\text{-}26)$$

Where

$$\tan\theta = \frac{2\delta\theta}{4\theta^2 - \varepsilon(\delta - \varepsilon)} \qquad (2\text{-}27)$$

And

$$\tan\psi = \frac{\varepsilon}{2\theta} \qquad (2\text{-}28)$$

The integration constants θ and ψ cannot be simply related to the parameters δ and ε but must be calculated by a trial and error procedure. For the finite current density in the electrode, $0 < \theta < \pi$.

The dimensionless reaction rate is found to be

$$\frac{dj}{dy} = \frac{2\theta^2}{\delta}sec^2(\theta y - \psi) \qquad (2\text{-}29)$$

Figure 2-15 shows reduced reaction rate for $\varepsilon = 0$ and $\varepsilon = \frac{1}{2}\delta$. From the graphs, it can be seen that for small values of δ the reaction is uniform, but for larger values of δ the reaction mainly takes place at the interfaces.

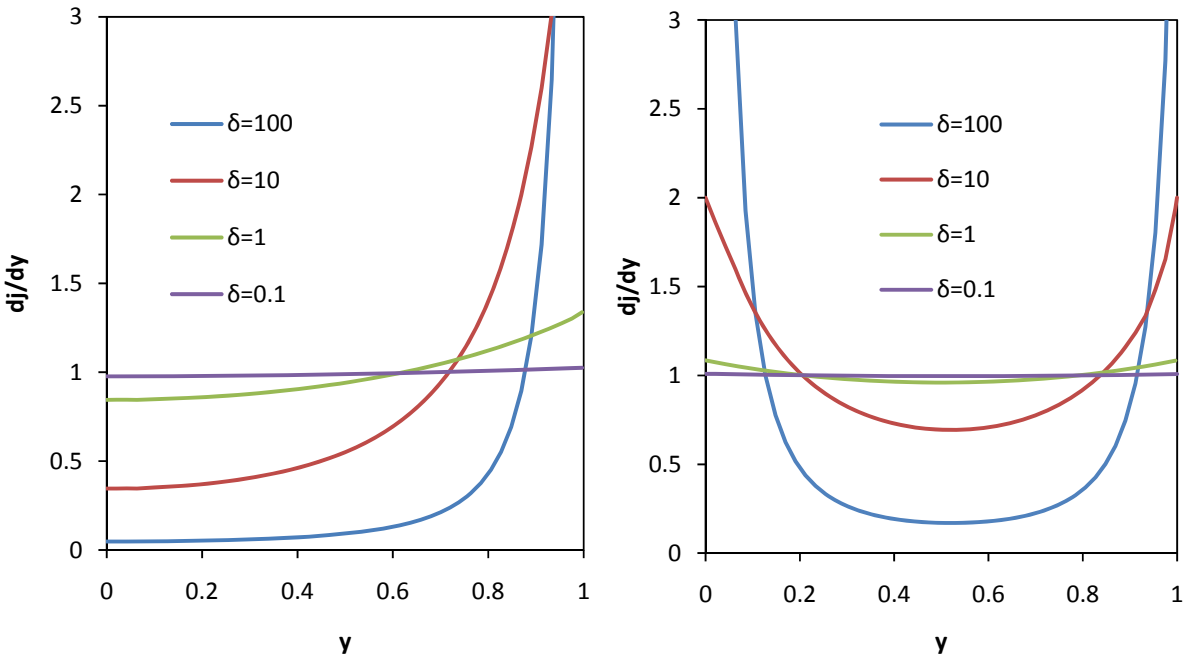

Figure 2-15 Reduced reaction rate distribution for Tafel polarization with a) ε = 0 and b) ε = ½δ

The potential of the metal backing plate can be calculated according to

$$\beta\Phi_1(L) = (\delta - \varepsilon)\left[\frac{\varepsilon}{\delta} + \frac{2}{\delta}\ln\sec(\theta - \psi)\right] + \frac{2\varepsilon}{\delta}\ln\sec\psi + \ln\left(\frac{2|I|\theta^2}{ai_0L\delta}\right) \qquad (2\text{-}30)$$

Where a is specific interfacial area per unit volume, cm^{-1} and i_0 is exchange current density in Tafel polarization, amp/cm^2 [33].

2.6 Experimental methods

2.6.1 Steady state polarization

Steady state polarization is a basic and straight forward electrochemical analysis method, in which the relation between potential and current is measured. This method is done either potentiostatically where a cell voltage is applied and current is measured, or galvanostatically where current is introduced to the cell and potential is measured. In order for the relationship to be at steady state, normally either a very slow scan or staircase type profile is used (see experimental section in reference [3] for more information). Steady state polarization

measurements include all polarization effects including the thermodynamic potential, the overpotential due to the surface reactions, ohmic losses and diffusion terms. The relation can be described by equation 2-12.

2.7 Scanning and transmission electron microscope

A scanning electron microscope (SEM) is a type of electron microscope that images a sample by scanning it with a high-energy beam of electrons. The electrons interact with the atoms that make up the sample producing signals that contain information about the sample's surface topography, composition, and other properties such as electrical conductivity.

The types of signals produced by an SEM include secondary electrons, back-scattered electrons (BSE), characteristic X-rays, and etc. Secondary electron detectors are common in all SEMs. The signals result from interactions of the electron beam with atoms at or near the surface of the sample. In the most common or standard detection mode, secondary electron imaging or SEI, the SEM can produce very high-resolution images of a sample surface, revealing details less than 1 nm in size. Due to the very narrow electron beam, SEM micrographs have a large depth of field yielding a characteristic three dimensional appearance useful for understanding the surface structure of a sample

Transmission electron microscopy (TEM) is a microscopy technique whereby a beam of electrons is transmitted through an ultra thin specimen, interacting with the specimen as it passes through. An image is formed from the interaction of the electrons transmitted through the specimen; the image is magnified and focused onto an imaging device, such as a fluorescent screen, on a layer of photographic film, or to be detected by a sensor such as a CCD camera.

TEMs are capable of imaging at a significantly higher resolution than other microscopes. This enables the instrument's user to examine fine details even as small as a single column of atoms, which is tens of thousands times smaller than the smallest resolvable object in a light microscope. TEM forms a major analysis method in a range of scientific fields, in both physical and biological sciences. For further SEM and TEM reading refer to Transmission Electron Microscopy by Williams and Carter [34].

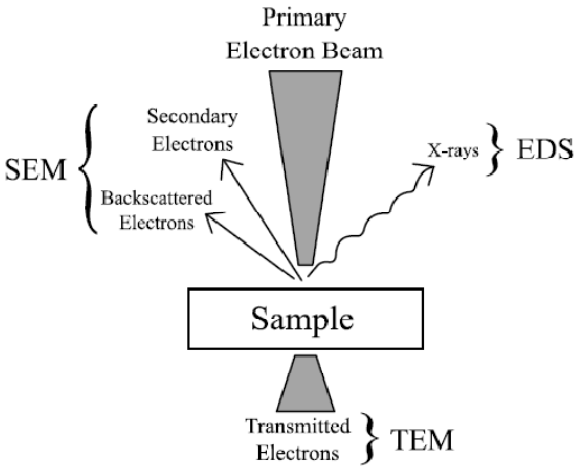

Figure 2-16 principles of electron microscopy [34]

3 Experimental

3.1 Equipments and chemicals

The chemicals and equipments that were used in this project are given in table 3-1 and 3-2

Table 3-1 List chemicals

Nafion®, 5wt% (95% deionised water), Alfa Aeser
Ir Black, Alfa Aeser
Iso-propanol, Merck
Hydrochloric Acid, Merck
Oxalic Acid, Alfa Aeser
ATO(Sb-doped SnO_2), Alfa Aeser

Table 3-2 List of apparatus

25cm^2 Water electrolysis Cell, Baltic Cell
Potentio Stat SP 150 , Bio Logic
Water pump520 S, Watson Marlow
20% Pt on Vulcan XC72 catalyst sheet, E-Tek
Airbrush Badger 360 USA

3.2 Catalyst synthesis

The course of the polyol synthesis used for synthesis of 20% Ir on ATO was as follows which was done by Katrine Dredvik and described in [35] :

0.1M NaOH in ethylene glycol (EG) was prepared by weighing out 0.20g of crushed NaOH pellets and dissolving it in 45ml EG in a three necked round bottom flask. The NaOH does not dissolve very easily in EG, so the solution was kept at 30°C and 400 rpm stirring until the NaOH was dissolved. The NaOH was dried at 105°C over night prior to this.

Ir-salt was weighed out and transferred to the NaOH/EG solution. The Ir-salt was weighed out and 5ml EG was added to it inside the glove box to avoid exposure to humidity. The dispersion was then added to the round bottom flask, and thus supplying the last 5ml of EG needed to make the 0.1 M NaOH/EG solutions.

The mixture was heated to 170°C and kept at this temperature for three hours under reflux and with N_2 gas bubbling through it. The stirring was set at 250rpm.

The mixture was cooled to 80°C. This took about 60 minutes.

450mg of antimony tin oxide (ATO) was weighed out and dried over night at 105°C. The dry ATO was then added to the round bottom flask through a funnel. The mixture was set at 400rpm stirring for 40 minutes. The pH was then adjusted to below 3 by addition of 1M H_2SO_4. The pH was measured both before and after adding the acid.

The mixture was set at 80°C and 250rpm stirring over night, still under reflux and with N_2 bubbling through it.

The heat was turned off and the mixture was set to cool for some time (just to make it possible to handle), still with reflux, stirring and N_2 bubbling.

The mixture was transferred to a plastic centrifuge tube and centrifuged at 8000rpm for 10 minutes.

The supernatant (EG) was decanted off and the product was washed in hot water. The mixture was put in an ultrasonic bath and shaken until the product was well dispersed in the water. The mixture was centrifuged again, and the washing procedure was repeated. The pH of the supernatant was measured after each washing and the washing procedure was repeated three times. The pH of the supernatant after the last centrifuging should be the same as the pH of the water used for the washing, about 5.

A small amount of water was added to the product (just enough to make the product disperse) and the mixture was transferred to a Petri dish, covered with perforated aluminum foil and dried at 105°C over night.

According to Dredvik master thesis [35] final catalyst was consist of 20wt% Iridium particles with diameter of 1-2 nm attached to ATO support with diameter of 20-30 nm.

3.3 MEA preparation

3.3.1 Nafion Membrane preparation

Nafion 115 membrane was pre cleaned in boiling water for 15 minutes, then boiled in 3% H_2O_2 for 30 minutes to remove organic impurities, after being washed with distilled water it was boiled in 0.5M H_2SO_4 for 30 minutes to exchange ions with protons, and again washed with

distilled water. Prepared membranes were boiled in distilled water for 15 minutes for three times and finally stored in distilled water until use.

3.3.2 Ink preparation

For each sample, according to table 3-3 different masses of the catalyst was weighed out and put in the sample holder. Different amounts of Nafion were added to each sample afterwards proportional to catalyst target loading to keep the weight percent of Nafion at 7.5 wt%. Then iso-propanol and water were added with the ratio of 2:1 respectively. Final fraction of iso-propanol in the ink was 75%. The efficiency of spraying assumed to be 65%.

Prepared inks were then ultrasonicated for 5 minutes and stirred at 2000 rpm for an hour.

3.3.3 Spraying and assembly

Prepared Nafion membrane was dried in the oven at 70°C for an hour between two sintered glass plates to avoid deformation during drying. Dried membrane was weighed out then mounted in a 5 cm^2 frame and put on the hot-plate at 85°C. The ink was carefully sprayed on the membrane using air brush shown in figure 3-1 then it was left on the hot-plate for 10 minutes to be dried. Then the membrane was put in the oven at 80 °C for 15 minutes to make sure there is no water remains in the catalyst layer to interfere weight measurement. The Membrane with catalyst was weighed out then subtracted to the membrane's weight to get the loading.

Figure 3-1 air brush used for spraying the catalyst

A 5 cm^2 E-tek sheet was put on the other side of the membrane as shown in figure 3-1a, in the way that the gas side faces away from the membrane and Pt side attaches the membrane. Then the assembly was put in the hot-press at 130 °C and pressed with 18 kg/cm^2 for 1 minute. Final MEA is shown in the figure 3-1b

Two sets of MEAs with loadings of 0.4, 0.6, 0.8 and 1.0 $mgcm^{-2}$ was prepared. Ink fractions and loadings are summarized in table 3-3

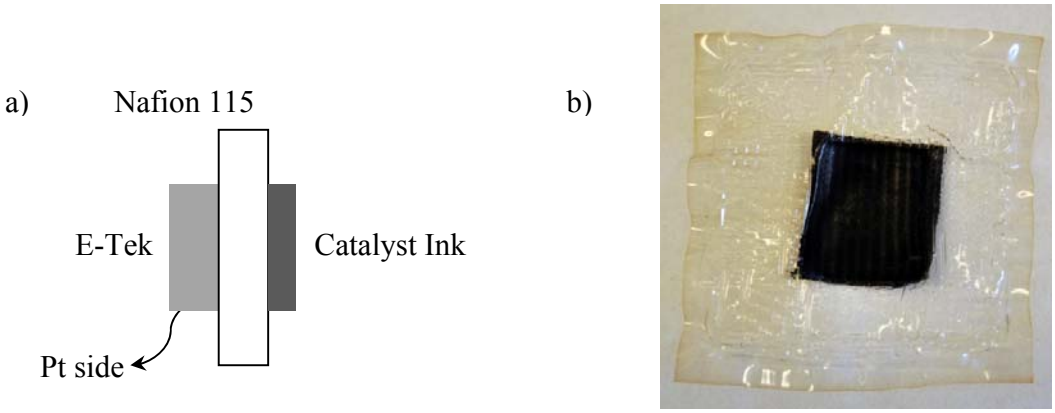

Figure 3-1a) MEA cross section b) final MEA after use

Table 3-3 Ink composition for different loadings

MEA number	Ir loading ($mgcm^{-2}$)	Nafion fraction (wt%)	Catalyst (mg)	Nafion solution (mg)	Iso-propanol (µL)	Water (µL)
1 – 2	0.4	7.5	15	24	427	182
3 – 4	0.6	7.5	23	37.4	640	243
5 – 6	0.8	7.5	28.8	46.8	800	342
7 – 8	1.0	7.5	38.5	62	1067	456

3.4 Washing titanium sintered plates

After running the Measurements, an oxide layer was seen to cover the titanium sintered current collectors. A drastic loss in performance was observed according to polarization curves shown in figure 3-3 by using the same MEA with different current collectors , this unwanted oxidation

resulted in not only unreliable data for comparison and degradation study but also practical issues about replacing current collectors with new ones after every measurement. Figure 3-4 shows oxidation of a plate compare to a new one, the 5 cm^2 square in the middle is referred to the place where the catalyst layer was placed.

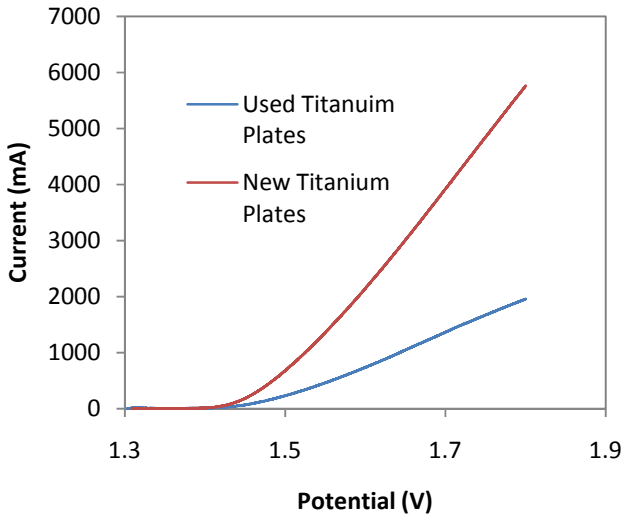

Figure 3-3 polarization curve for the same MEA but with used and new titanium current collector

To solve the problem porous plates were left in 10 wt% oxalic acid at 80 °C for 2-3 hours and then sonicated for 10 minutes in hydrochloric acid to remove titanium oxalate, then washed completely with distilled water to avoid hydrochloric acid to enter our electrolysis system. But this was still a temporary plan to avoid buying new plates, because during long experiments it was not possible to conclude if the loss is due to catalyst degradation or plates' oxidation. After all, to evade oxidation, a 100 nm gold layer was coated on the washed plates. Gold coated titanium porous plates, in addition to prevent fast oxidation, result in higher performance of the cell which is thought to transpire because of lower contact resistance of gold-Iridium and higher number of contact points. Since degradation or corrosion of the current collectors is not the objective of this work, therefore no further exploration was carried out.

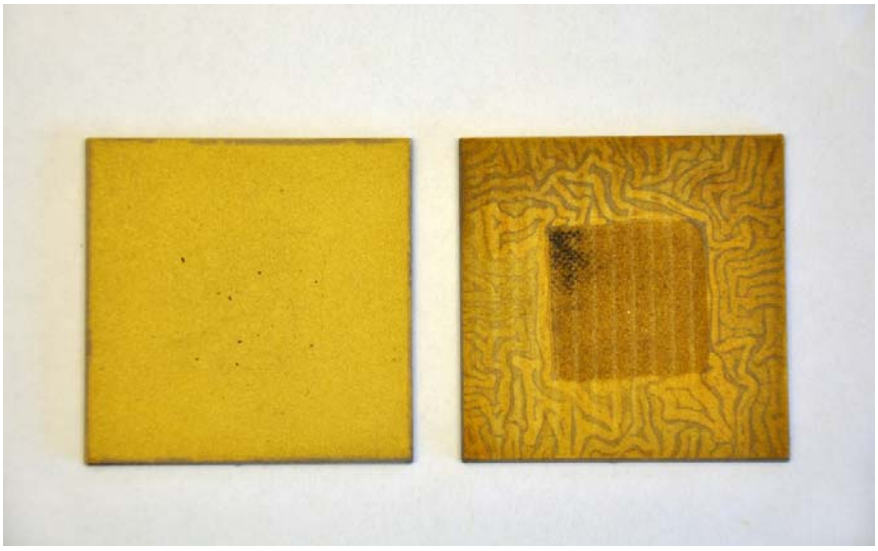

Figure 3-4 New and used gold coated titanium current collectors

3.5 Electrochemical tests

3.5.1 Polarization

Baltic fuel cell setup was used for electrochemical tests such as steady-state polarization and cyclic voltametry. Figure 3-5 shows the water electrolysis setup. Water flow was set to 238ml/min using Water pump520 S, Watson Marlow. Polarization was performed between 1.3 to 1.9V with the scan rate of 10mV/s. EC-lab software was used for testing and recording data, and Potentio Stat SP 150 20V/20A, Bio Logic was connected to the cell.

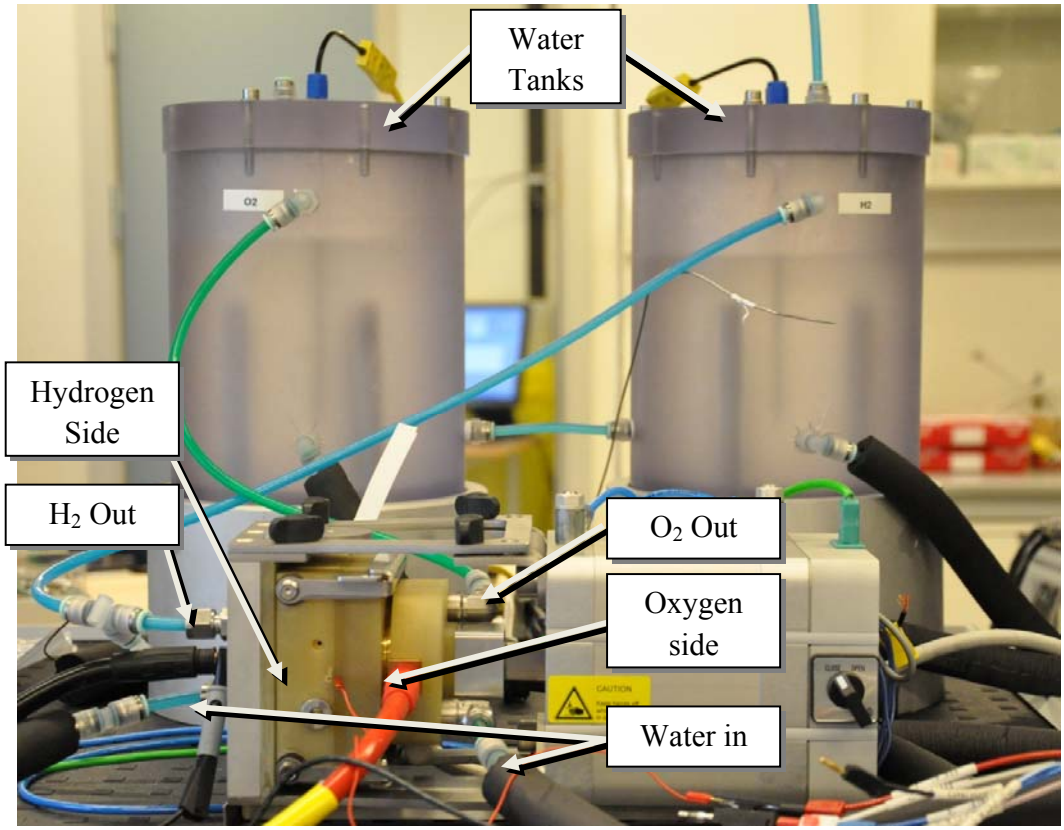

Figure 3-5 water electrolysis setup

3.5.2 Accelerated degradation test

To accelerate degradation, instead of keeping the MEA at constant current and measure the potential, the current was kept at 100 mA/cm^2 10 minutes and then 700 mA/cm^2 for another 10 minutes. This cycle was continued for 72 hours and every 10 hours a polarization was performed. The cycle is shown in the figure 3-6.

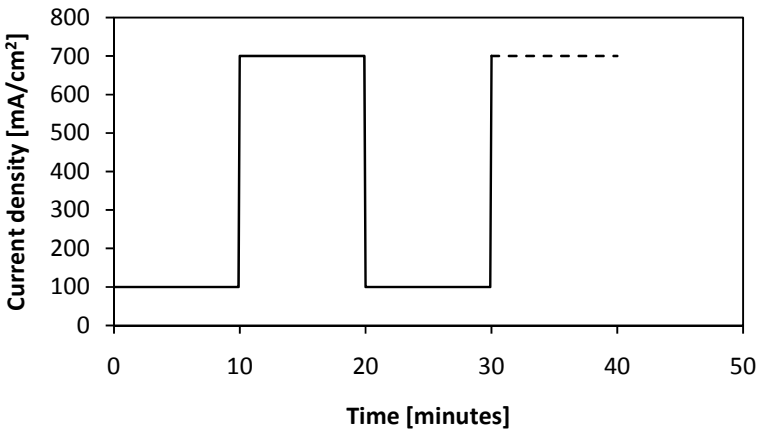

Figure 3-6 current density cycle for the accelerated degradation test

3.6 Scanning and transmission electron microscopy

To study cross section of the MEAs , Hitachi S-3400N, LV SEM was used. First carbon cloth on the hydrogen side of the electrochemically tested MEAs with different loading was piled off then MEAs were put in the liquid nitrogen for 30 seconds. They were broken afterwards to get randomly selected areas and avoid cutting which may associate with deformation or change in the catalyst layer.

To study the cross section of the MEAs with JEOL 2010F, FEG TEM, first the carbon cloth on the hydrogen side was piled off, the MEA was put in the epoxy left to be dried then it was cut into pieces and delivered to Sintef co. TEM responsible. Final TEM sample preparation and microscopy was done by Per Erik Vullum.

4 Result and discussion

4.1 Catalyst structure and performance

Figure 4.1 shows a TEM image of the oxygen catalyst used in this work comprising of small Iridium particles (1-3 nm), attached to larger ATO particles (20-25 nm). Some agglomeration of the small Ir particles is visually obvious, with larger areas of the ATO support surface essentially empty of Ir catalyst. The uneven distribution of Ir catalyst may suggest variations in the active surface area and thus also in the performance.
However, steady state polarization measurements showed a promising performance of 2.1 A/cm^2 at 1.85 V with a loading of 0.8 mg/cm^2 at 80 degrees C, which is about 40 % better than the commercial MEA tested in the same cell with the same operating conditions

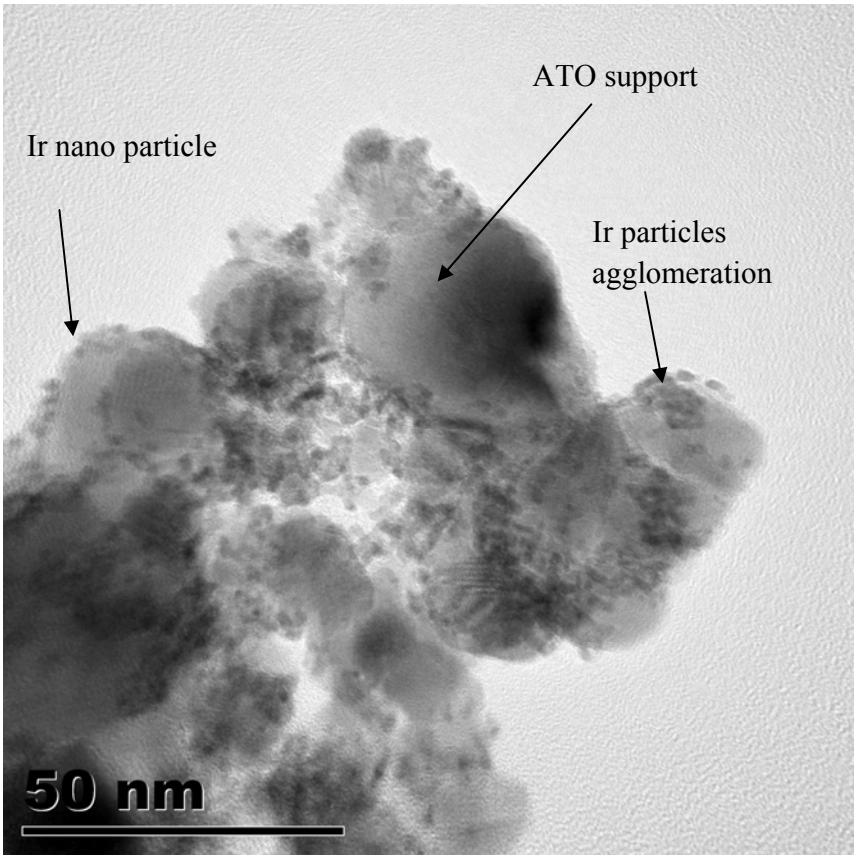

Figure 4-1 TEM image of the catalyst powder

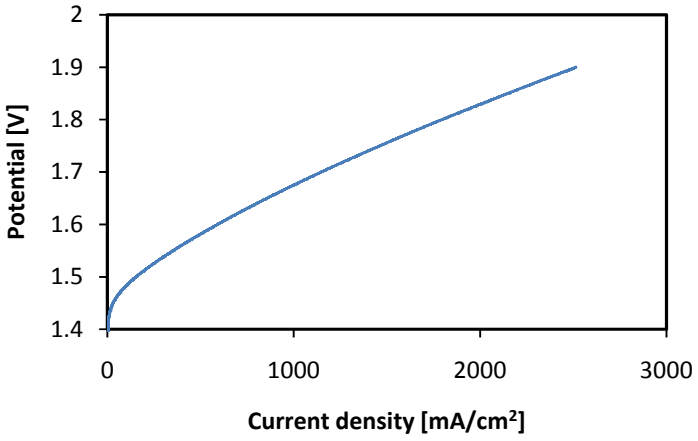

Figure 4-2 polarization curve for an MEA with 0.8mg/cm^2 loading

4.2 Effect of loading on layer thickness and cell performance

4.2.1 Layer thickness

Scanning electron microscope was used to study the cross section of the MEAs. For loadings 0.4, 0.6, 0.8 and 1.0 mgcm^{-2}, mean thicknesses of 2.0, 3.1, 4.7 and 5.4 µm were measured respectively. SEM images are shown in figure 4-3. Cross section images for loadings of 0.4 and 0.6 were taken in back scatter mode where the heavier elements (Iridium in this case) shines up and catalytic layer is more distinguishable. Catalyst layer was relatively uniform with the range of 0.5 µm higher or lower than the mean layer thickness.

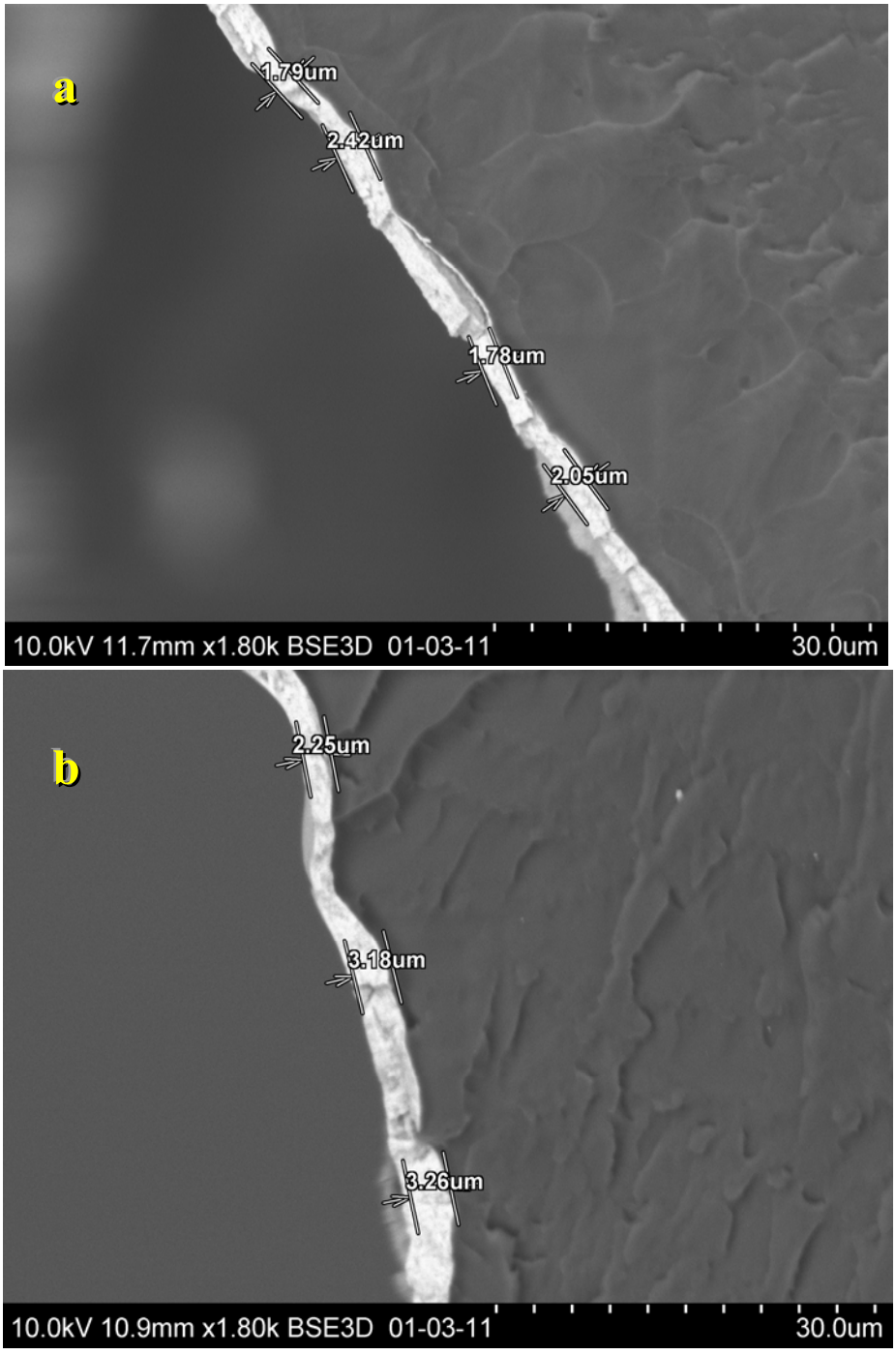

Figure 4-3 cross section of the MEAs' oxygen catalyst side with different loading a) 0.4mg/cm^2 b) 0.6mg/cm^2

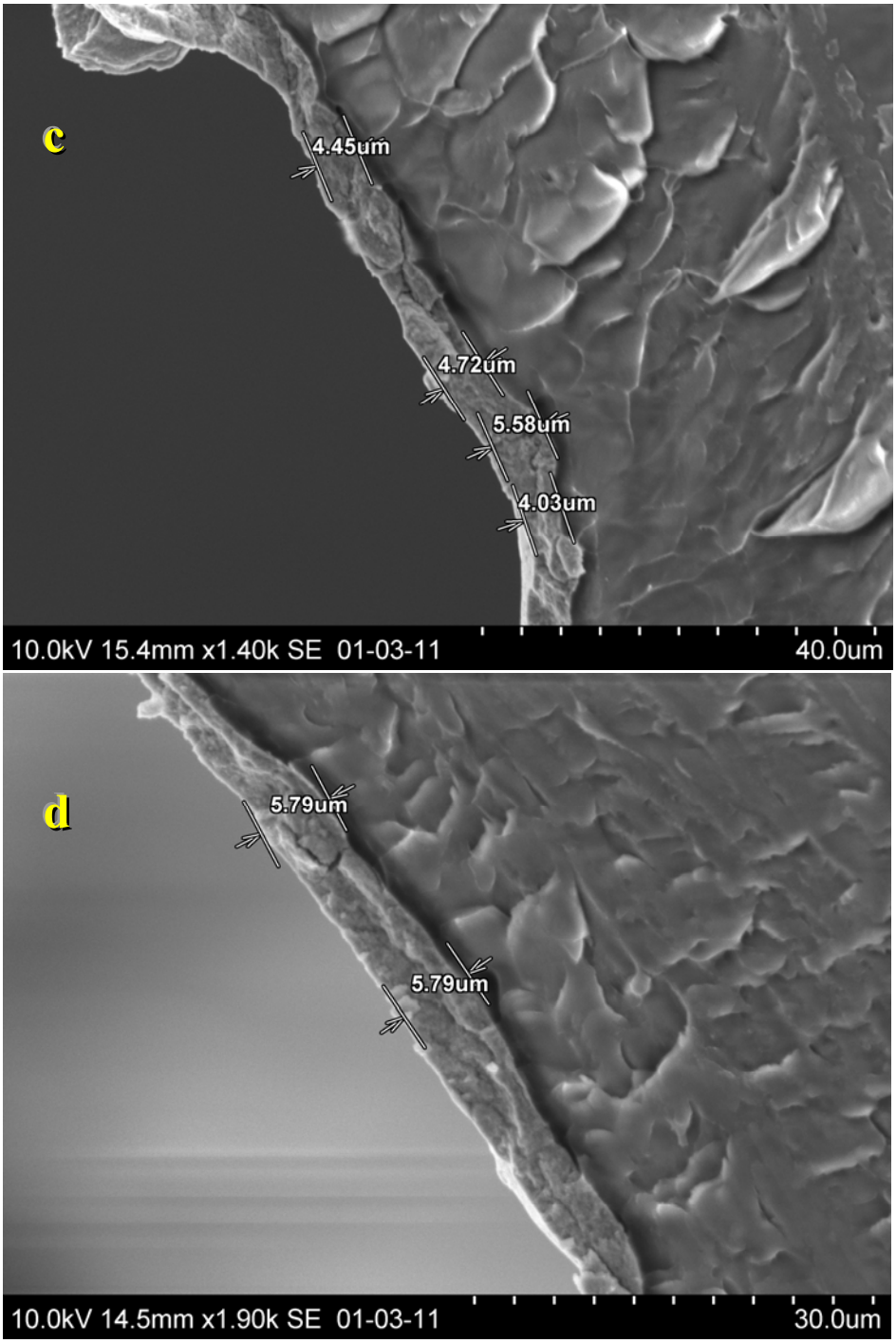

Figure 4-3 cross section of the MEAs' oxygen catalyst side with different loading c) 0.8mg/cm^2 d) 1.0mg/cm^2

The incident electron beam density increases with magnification and would result in damaging (burning) of the surface structure due to the high resistivity of Nafion. A linear relationship

between loading and layer thickness was found as shown in figure 4-4 in which R-squared of the linear trendline is 0.982.

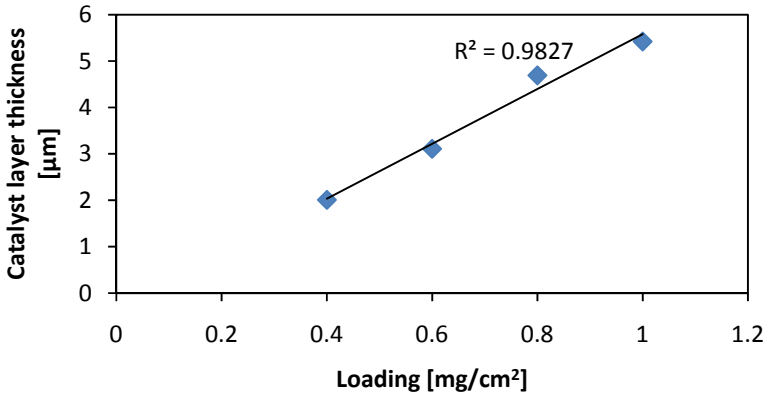

Figure 4-4 catalyst loading vs. layer thickness

4.2.2 Cell performance

Steady state polarization was performed to measure the performance of the catalyst layer. The results showed that at low potentials an increase in loading and layer thickness resulted in higher currents at certain potential. Figure 4-5 shows current density versus loading at 1.45 V. Two sets of experiments was performed; as it can be seen in the figure there is an unexpected deviation at 0.8mgIrcm^{-2} for the second set so it is not taken into consideration. It is regarded as a result of either human error in the MEA preparation or cell assembling, or unanticipated artifacts from the measuring equipment, which seems to be most prominent in the low current density potential region. A more plausible explanation is a thicker membrane, giving improved performance at low current density compared to higher. At low overpotentials, the current density is said to be under activation control [36], thus an increase in active surface area will increase the total current accordingly. Higher loadings and layer thickness means higher active surface area and more sites for the reaction to happen [37]. Accordingly, the total current increases with loading at a given potential. Figure 4.5 shows the responding current density (geometric) at 1.45 V as a function of catalyst loading.

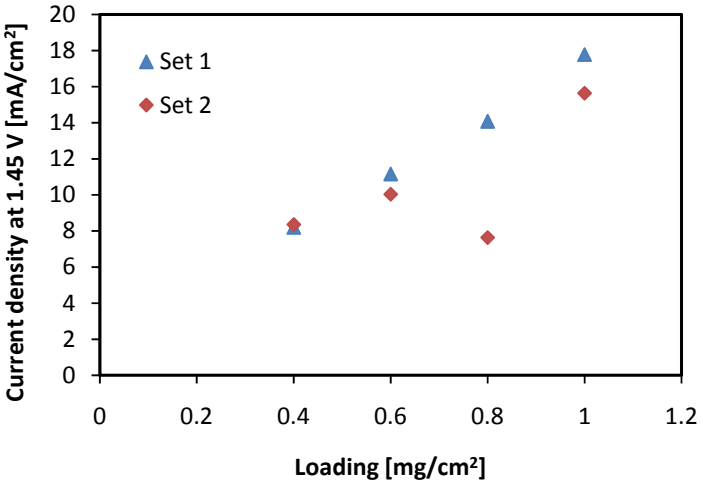

Figure 4-5 current density versus loading at 1.45V

Figure 4-5 shows current density versus loading at 1.65V where reaction is likely to be mixed controlled, both kinetics and mass transport have effect on the reaction rate which means even though there are a lot of active sites for the reaction to happen, mass transport to or from the sites struggle to keep up with the rate of reactions. Moreover in these potentials the ohmic part of the equation 2-12 is becoming more prominent. This may be the sole reason why a current drop can be seen for set 2 at 1.6 V (figure 4-6).

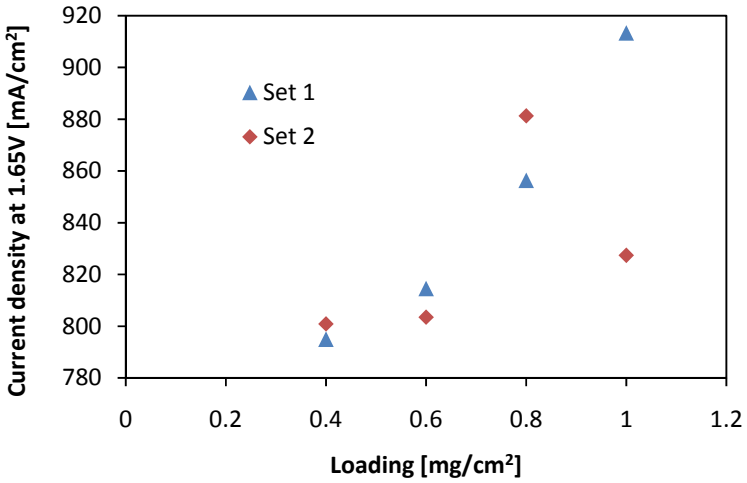

Figure 4-6 current density versus loading at 1.65V

At high potentials ohmic drop plays an important role because current is high which makes the IR part in the equation 2-12 higher than the rest which follows equation 2-14. On one hand higher loading means more active surface area and higher cell current due to higher number of active sites, on the other hand by going to high loadings the resistivity of the layer increases and ohmic loss may be significant. Consequently, a maximum in current density vs. loading would

be expected. This can also be seen from the experimental results displayed in figure 4.7, which shows current density at 1.85V versus loading.

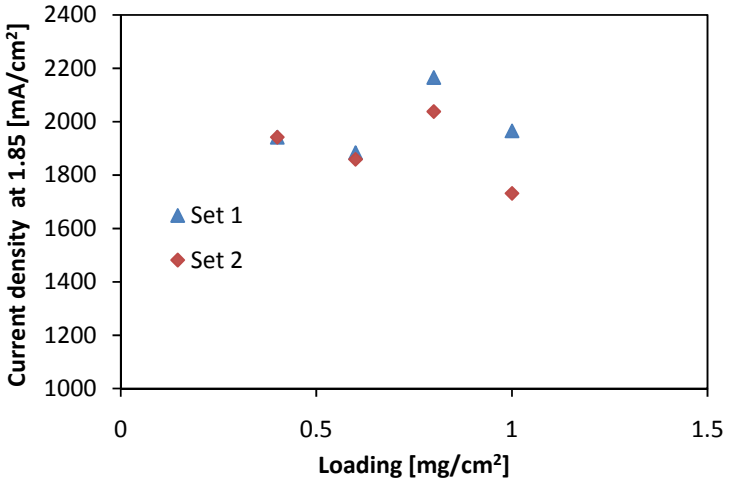

Figure 4-7 current density versus loading at 1.85V

As it can be seen in figure 4-7 at 1.85V, 0.8 mg/cm^2 shows the best performance and highest current density among the others. It should be said that if the current is normalized to mass of Iridium, the lowest loaded MEA shows the best utilization of catalyst with respect to Iridium mass. This could be in consequence of low thickness that allows all the catalyst to be able to include in reaction. However, the total production is more important for industrial cells, not production per unit mass of iridium. Iridium mass is not the only factor in the cost, low total current density per cell result in adding more cells for the same amount of production which can affect the feasibility of a project. Figure 4-8 shows current per mg of iridium versus potentials for different loadings.

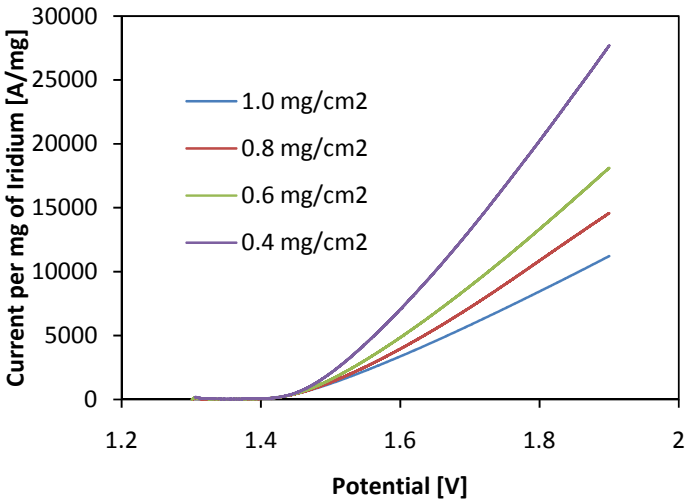

Figure 4-8 current per mg of iridium versus potentials for different loadings

4.3 Theoretical analysis of current distribution in catalytic layer

4.3.1 Effect of different variables on the theoretical model

Porous electrode was modeled with the help of Newman et al. [33] analysis. This model can describe current distribution and reaction rate in the porous layer using layer thickness, Tafel slope, total current density, electron conductivity of the catalyst and proton conductivity of the layer as result of presence of Nafion. Using equations

$$\frac{dj}{dy} = \frac{2\theta^2}{\delta} sec^2(\theta y - \psi) \qquad (2\text{-}22)$$

and

$$j = \frac{\tan(\theta y - \psi) + \tan(\psi)}{\tan(\theta - \psi) + \tan(\psi)} = \frac{2\theta}{\delta}\tan(\theta y - \psi) + \frac{\varepsilon}{\delta} \qquad (2\text{-}26)$$

described in theory section chapter 2.5.1 and putting the cell's total current 2.1 A/cm^2 at 1.85V, depends on conductivities we may get reaction rate and current distribution through the layer with different loadings from 0.2 to 1.2 mg/cm^2 as shown in figure 4-9. Higher proton conductivities relative to electron conductivity results in most of the reaction to happen near current collectors at *y=0* (figure 4-9), in contrast lower proton conductivities than electron conductivities results in low, or limited reaction near current collector (figure 4-10). In addition it can be seen that by decreasing the layer thickness (loading), reaction tends to take place uniformly through the plane. Therefore lower thicknesses (loadings) show better utilization of the catalyst since there is no part of the layer with very low reaction rates which also support the author's reasoning for the MEA with lowest loading (thin layer).

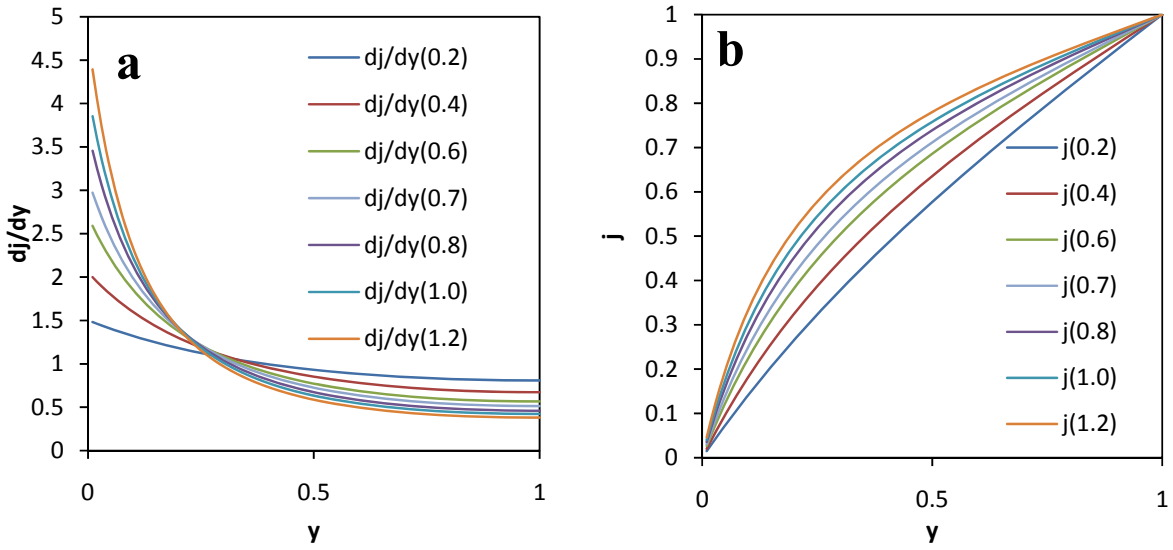

Figure 4-9 a) reaction rate and b) current distribution through the catalytic layer with high proton conductivity

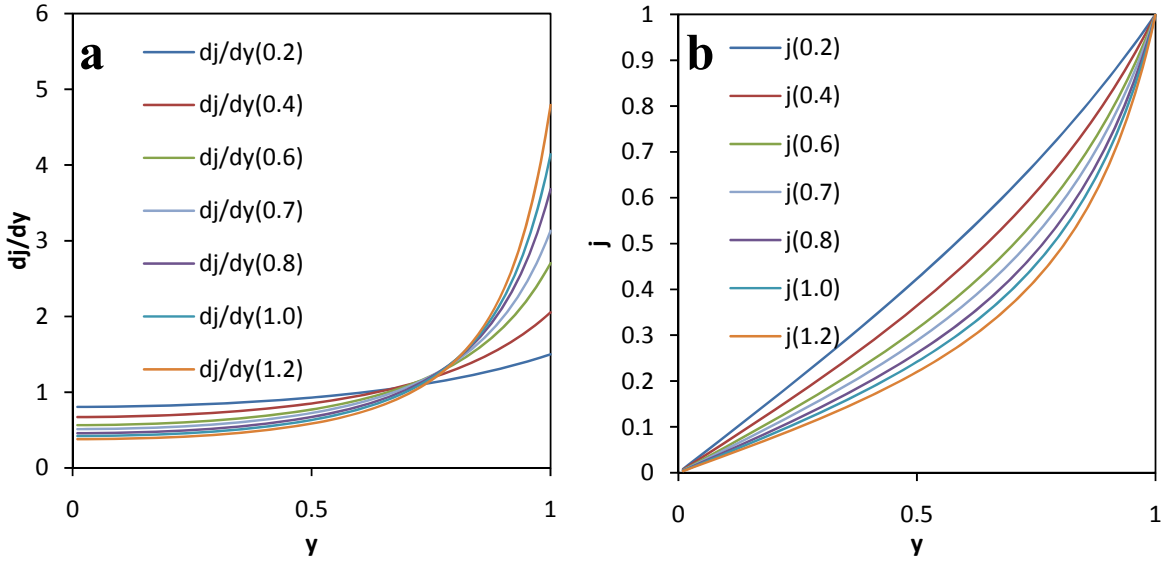

Figure 4-10 a) reaction rate and b) current distribution though the catalytic layer with high electron conductivity

Potential at the backing plate is calculated by equation

$$\beta\Phi_1(L) = (\delta - \varepsilon)\left[\frac{\varepsilon}{\delta} + \frac{2}{\delta}\ln\sec(\theta - \psi)\right] + \frac{2\varepsilon}{\delta}\ln\sec\psi + \ln\left(\frac{2|I|\theta^2}{ai_0L\delta}\right) \qquad (2\text{-}30)$$

It can be presented versus the thickness of the layer. This potential represents overpotential; by adding reversible potential to it we can show total cell voltage. For this value more variables like specific interfacial area per unit volume and exchange current density are important in put parameters in the calculation. Figure 4-11 shows potentials at 2.1 and 0.01 A/cm^2 versus layer thickness, where Tafel slope is assumed to be 30mV/dec [35], Nafion conductivity is 0.02 S/cm [31], catalyst conductivity is assumed to be the same at ATO conductivity 0.008 S/cm, specific interfacial area per unit volume is 0.0005 cm^{-1} [37] and exchange current density is 0.05 A. There is a minimum in 3-4 µm for 2.1A/cm^2 but there is not a big change in potential by increasing the thickness of the layer.

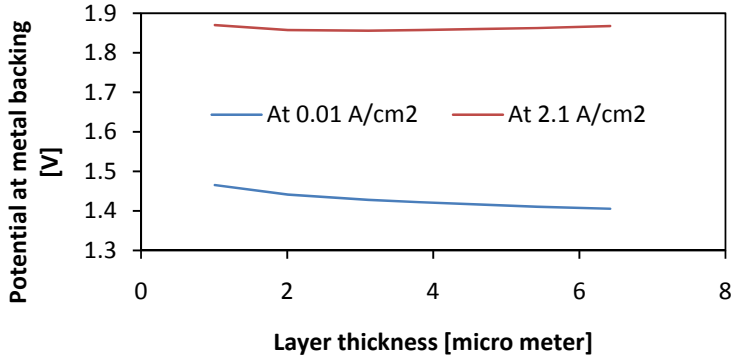

Figure 4-11 shows potentials at 2.1 and 0.01 A/cm^2 versus layer thickness

4.3.2 Experimental data and comparison with the model for porous electrodes

Putting experimental values shown in table 4-1 in the model's equations (these values were obtained according to appendix A-1) reaction rate and current distribution through the layer for different loadings are shown in figure 4-12 for 0.02 A/cm^2 and figure 4-13 for 2.1 A/cm^2. Measurement of the catalyst conductivity is described in appendix. Nafion proton conductivity chosen to be 0.02 S/cm in accordance to figure 2-9.

Table 4-1 experimental values for different variable

β	L [µm]	I [A/cm^2]	σ [s/cm]	κ [s/cm]	i_0 [A/cm^2]
32	4.6	2.1	0.02	0.8	0.05

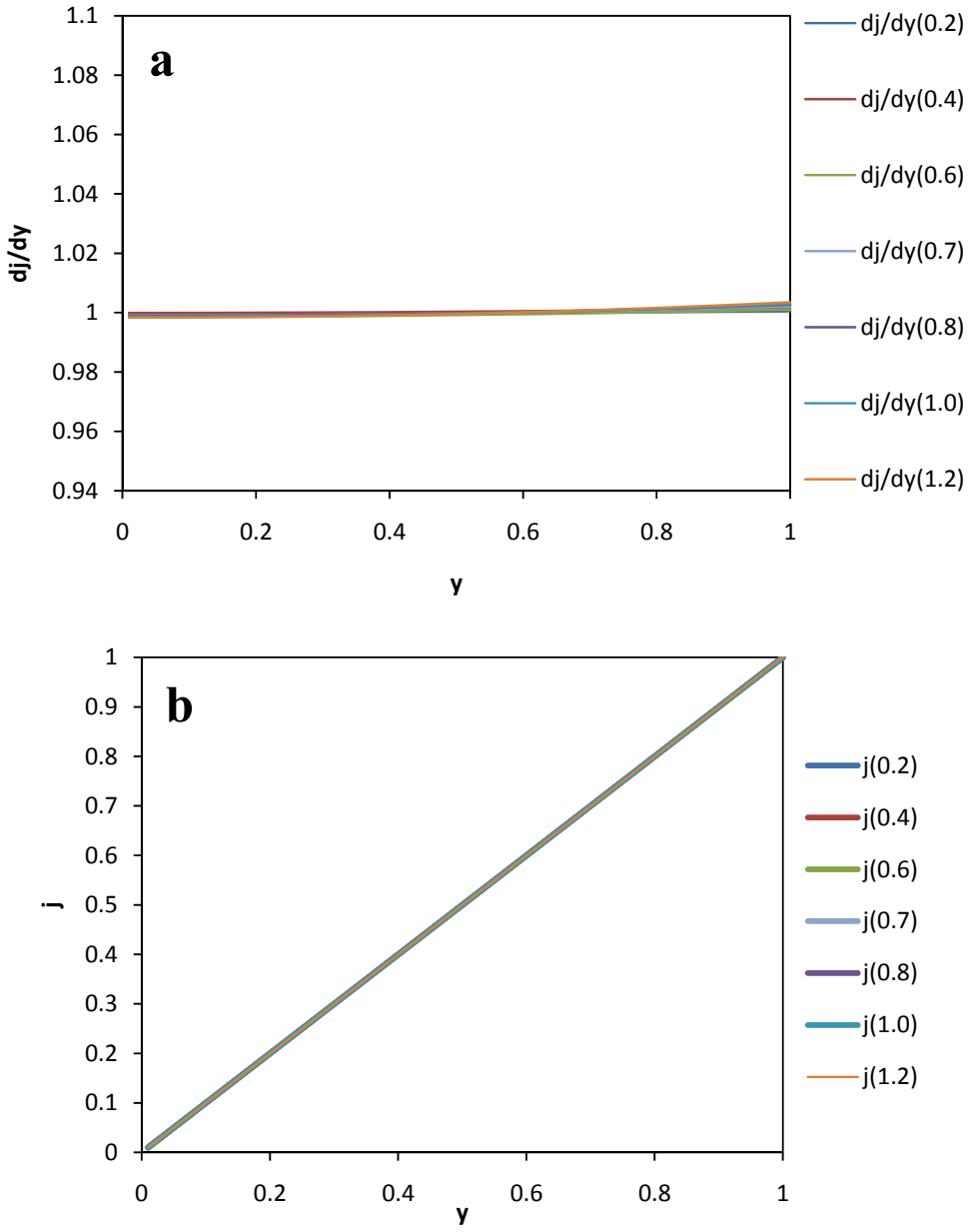

Figure 4-12 a) reaction rate and b) current distribution though the catalytic layer for 0.02A/cm^2

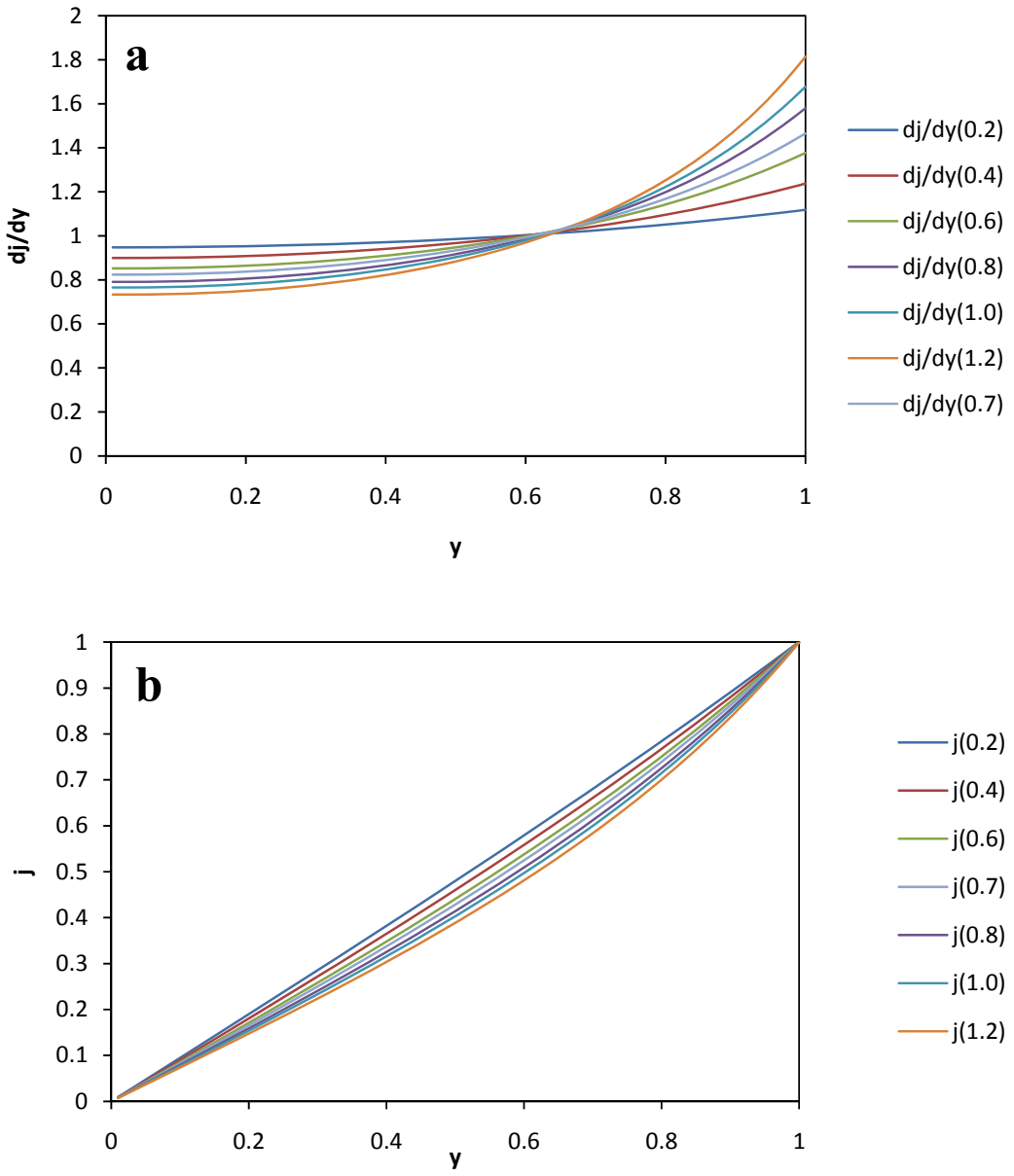

Figure 4-13 a) reaction rate and b) current distribution though the catalytic layer for 2.1A/cm^2

As it can be seen in the figures above, at low currents, reaction rate through the layer is quite uniform which means all the layer take part in the reaction and current distribution is a straight line. At low currents reaction is just kinetic control and mass transport or layer thicknesses are not having major effect on the curves shapes. It is also proved by the model that at low currents if proton conductivity σ or electron conductivity κ is changed the shape of the reaction rate and current remains constant means it is fairly independent of those at low currents. This means the reaction happens slow enough that transport of protons and movements of electron can keep up with the reaction and they are not rate determining factors.

On the other hand, at high currents, conductivities and layer thickness play a significant role on current distribution and reaction rate in which the kinetics are high and other factors like proton transport should keep up with the electrochemical reaction. In addition, figure 4-13 shows that most of the reaction tends to take place near the membrane especially at high loadings (thick layer), however for low loading reacting rate is uniform through the layer.

The best way to compare theoretical model and experimental data is using cell voltage at constant currents for different layer thicknesses. It gives us an idea if the model works in practice or needs any correction. At low currents they are fairly similar as shown in figure 4-14.

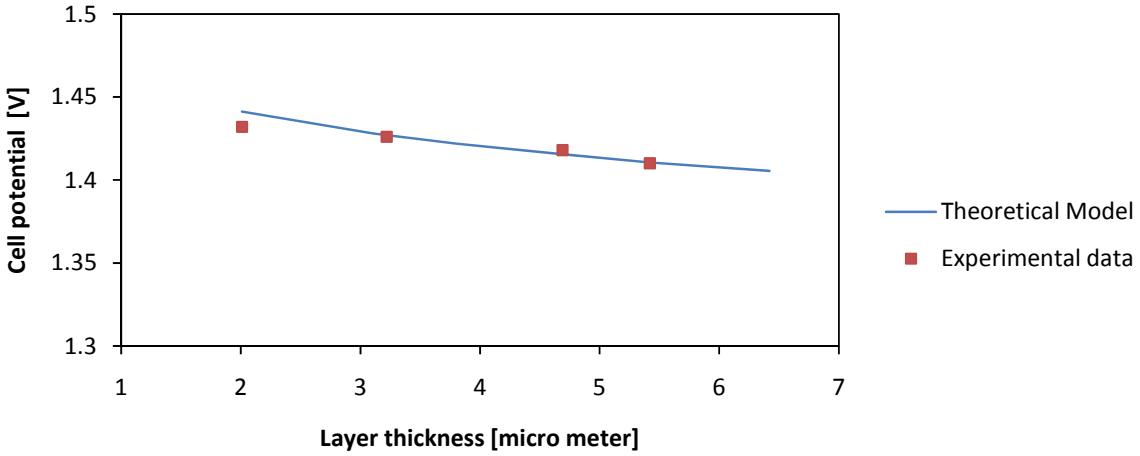

Figure 4-14 Cell potential versus layer thickness at 0.02A/cm^2

In contrast, for high currents the story is somewhat different. Looking deeply into the contact points between porous current collector and catalyst layer together with current paths through the layer (schematic view is shown in figure 4-16) one can see that the system is not perfect and some parts of the catalyst is not being used. This is because the porous current collectors have the particle size of 75 µm but the layer's biggest particles are 50nm. As shown in figure 4-16, this fact is more important when catalyst layer is thinner so the specific active area per volume, a, needs a correction factor for lower thicknesses. Assuming a linear relationship between thickness and a, and also $a_{eff} = a.\eta$ where η (correction factor) is one for our highest loading and 0.4 for our lowest loading. Corrected model is shown in figure 4-15. It is suggested that for the future works a thin layer of stable conductive material like highly graphitized carbon is sprayed on the catalytic layer so the in-plane conductivity in the layer can result in higher number of contact points and avoids any part of the catalyst to be unused. The Idea behind this proposal is the significant increase in performance by coating titanium sintered plates with gold which was a solution to avoid corrosion of sintered plates.

That is to say, the reason why this model cannot predict a minimum in cell voltage versus layer thickness is that the model was developed based on Tafel polarization, therefore phenomena like

mass transport and in-plane resistivity has not been taken into consideration. In addition, conductivity of the catalyst is measured when it has not been used. It is known that starting the reaction, Iridium is changed to Iridium oxide and the conductivity changes, which may imply further deviations between theory and practice. Last but not least, all the equations were solved for a one-dimensional electrode neglecting in-plane distributions, for the future works the equation can be solved for two or three dimensions.

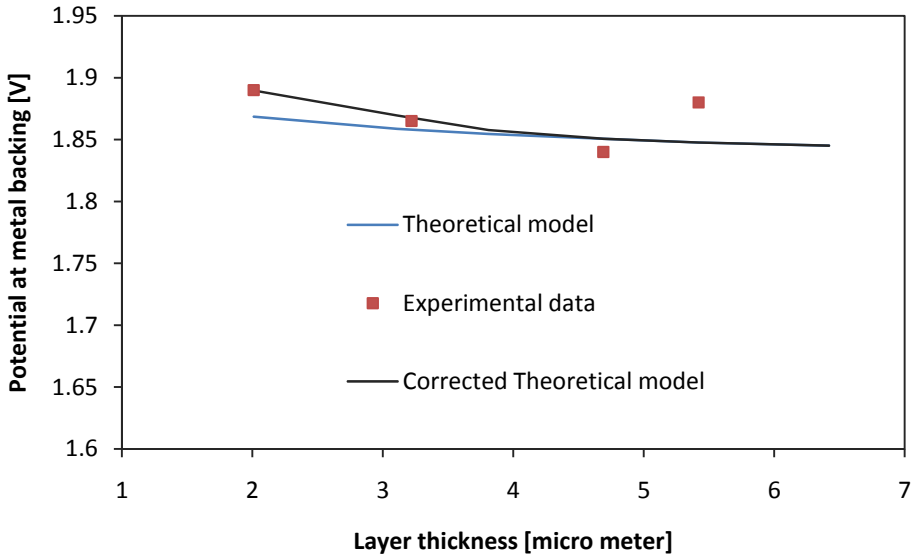

Figure 4-15 Cell potential versus layer thickness at 2.1A/cm^2

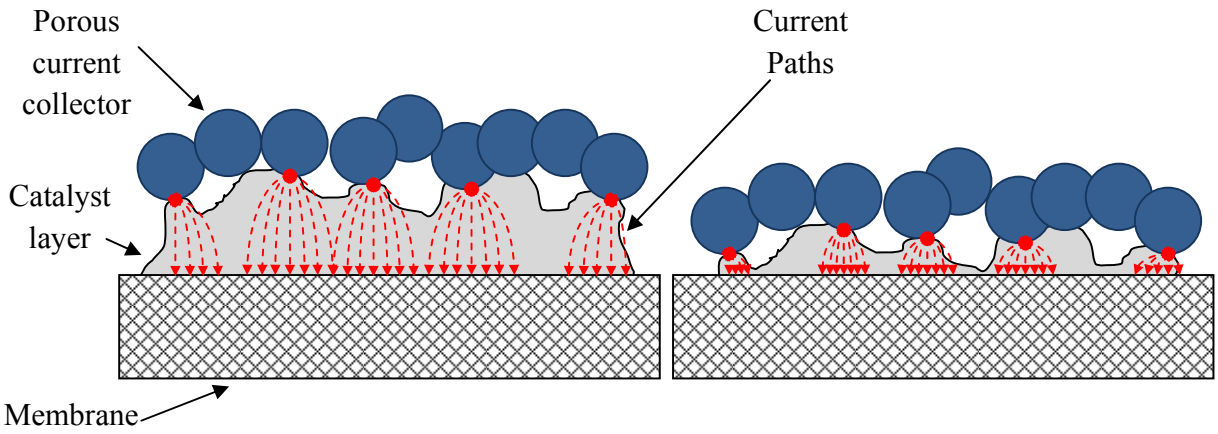

Figure 4-16 schematic view of contact points between porous current collector and catalyst layer showing the current flow in the layer

4.4 Degradation of the MEA

The durability of the optimized catalyst has also been tested using the protocol explained in the experimental section, and showed in the figure 4-17. The potential raised from 1.62 to 1.64V at 700 mA/cm^2 which is about 1.7% loss in performance after 72 hours. Since Iridium and Platinum nano sized particles at the surface of the ATO and carbon support have high specific surface area energy due to their small size, they tend to agglomerate/sinter at the harsh condition and high potentials during working cycles [39].

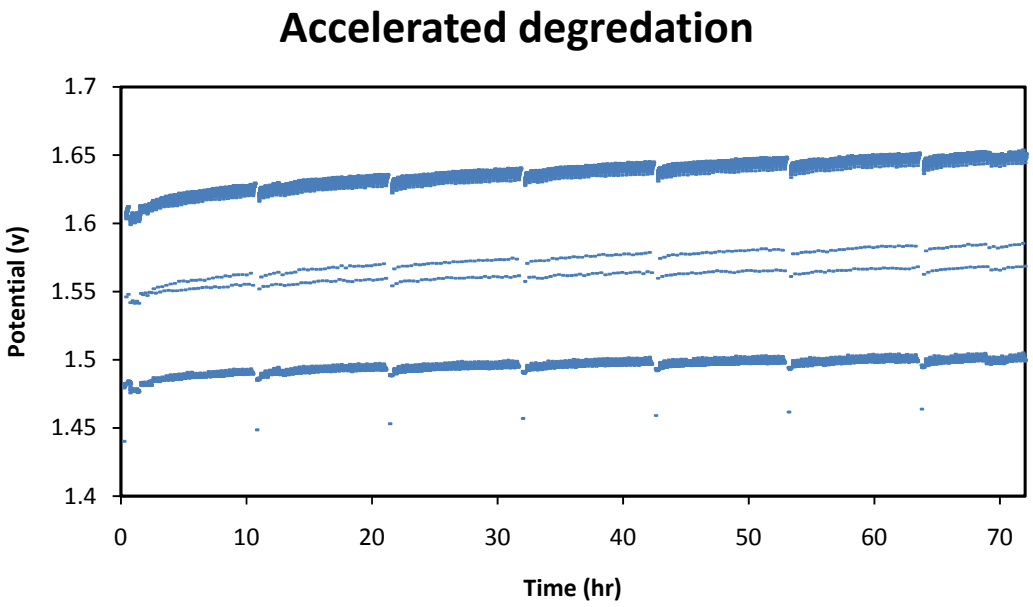

Figure 4-17 potential versus time for the degradation test explained in the section 3.5.2

Agglomeration of the particles decreases the electrochemical surface area of catalyst and consequently, the performance of the PEMWE degrades. However more importantly detachment of the catalyst from the support and its migration result in a major effect on degradation, this statement is highly supported with cross-section TEM images of an MEA after 72 hours accelerated degradation test. Figure 4-18 shows TEM images after 72 hours; a) migrated Iridium agglomerations can be seen in the membrane and also b) high concentration of Iridium can be seen agglomerated close to membrane at higher magnifications. Assuming reaction rates shown in figure 4-13 a, reaction happens closer to the current collector than membrane therefore degradation is highly affected by transport of ions in the catalytic layer. The driving force for transport of Iridium ions is potential gradient through the layer and the membrane (migration). Millet et al. [39] also pointed that the loss in performance can be related to the polymer: at high

current density, uneven distribution of current lines may lead to the formation of hot points and uneven membrane swelling. In addition, deposition of different metallic ions on the membrane can block channels and have effect of performance which in our case is of importance since traces of gold was found on the membrane after long term testing.

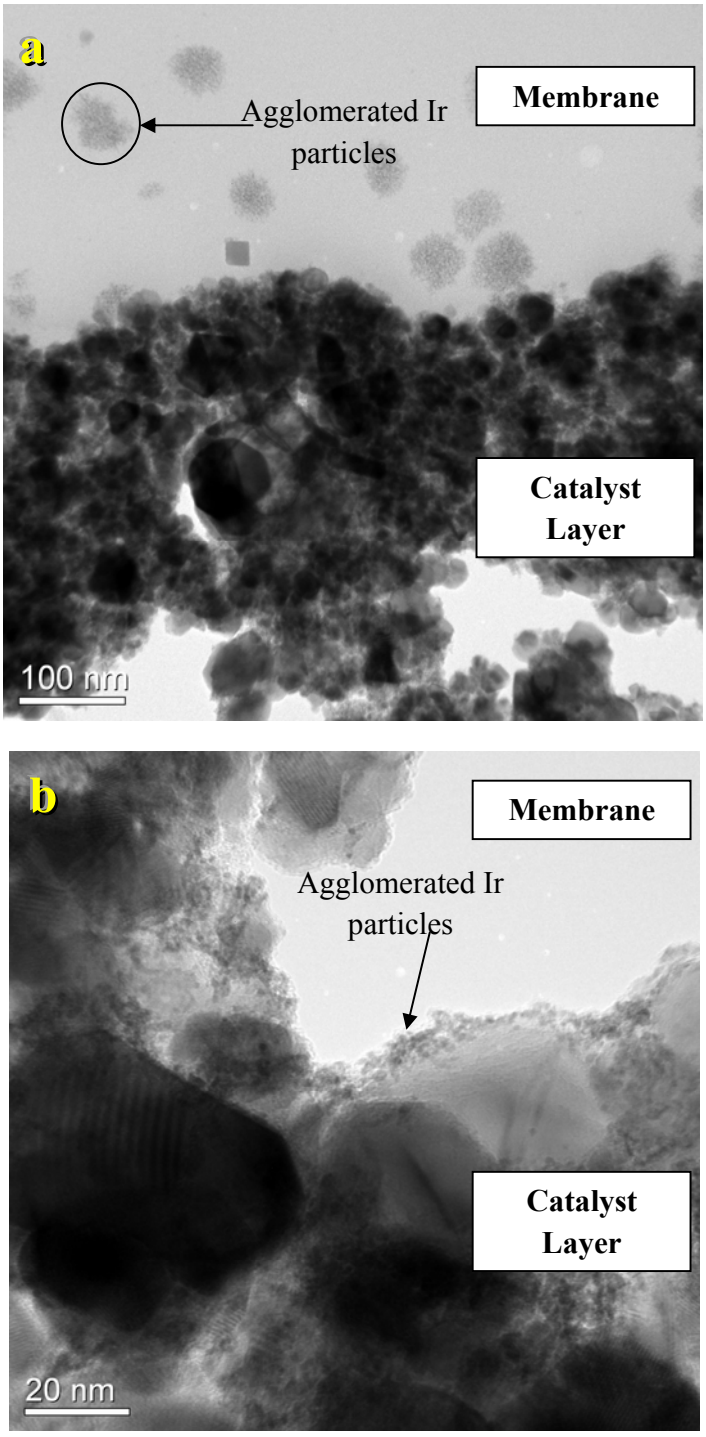

Figure 4-18 TEM images after 72 hours; a) lower magnification b) higher magnification

In addition, both anode and cathode are operated at low pH and high temperature (80°C) so the corrosion of both side current collectors is predicted. The oxide layer formed take part in increasing the ohmic resistance. According to

$$U_{cell} = E^{rev} + \eta_{anodic} + \eta_{cathodic} + IR$$

At high currents IR part is dominating and the slope of polarization curve can approximately demonstrate the ohmic resistance R. Figure 4-19 shows polarization curve, the slope from 1.84 to 1.9V represents resistance of the cell. Using this resistance, we have the opportunity to subtract the loss in relation to ohmic losses (oxidation of current collectors, ohmic drop in wires and etc) from the total loss, to obtain the loss which is only associated with the catalyst migration and agglomeration.

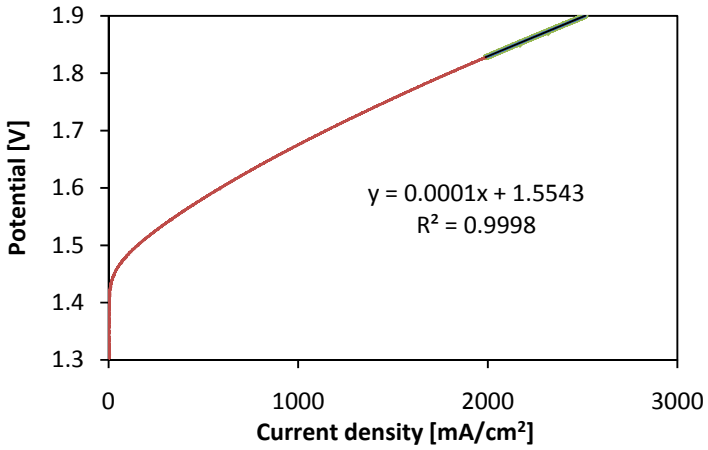

Figure 4-19 shows polarization curve for 0.8mg/cm^2 loaded MEA

To perform such normalization, resistance (R) was obtained from polarizations which were done every 10 hours during accelerated degradation test, and ohmic loss was subtracted from the total cell potential using 3500mA for cell current. The result is shown in figure 4-20. It can be seen that the rate of degradation was reduced from 0.5 to 0.3mV/hr; this means approximately 25% of the loss is from oxidation of the current collectors or other ohmic drops. Comparing these accelerated degradation results to previous litterateurs [40] which reported 1.2mV/hr as rate of loss for holding the catalyst layer at constant current confirms that our optimized catalyst is much durable, and promising in this context.

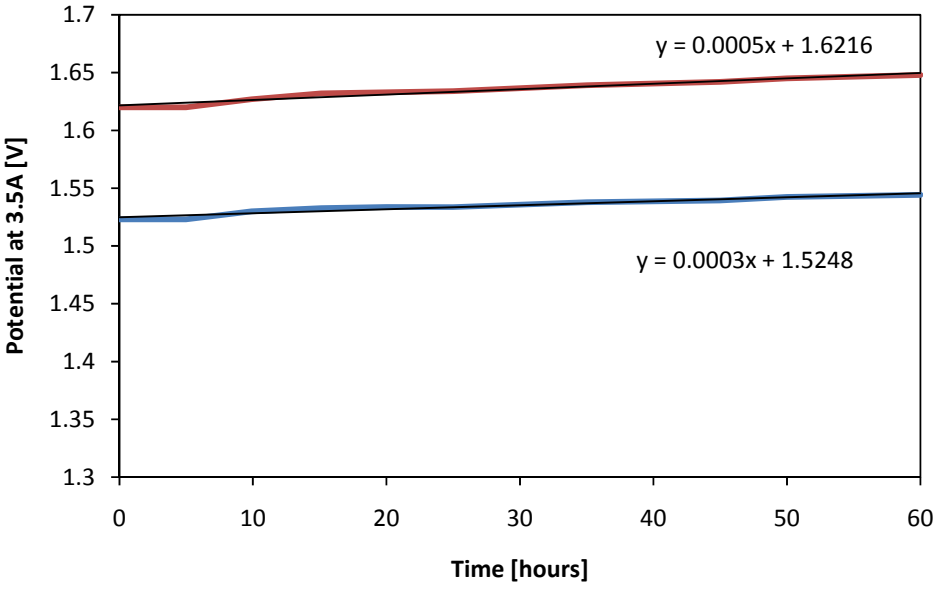

Figure 4-20 potential versus time for the degradation test explained in the section 3.5.2

5 Conclusions

To obtain a durable, high performing and affordable MEA, effect of loading (from 0.4 to 1.0 mgIr/cm^2) on the performance of the oxygen evolution catalyst at different potentials was investigated The catalyst layer being studied here comprised of 20 wt% Iridium on Antimony Tin Oxide (ATO) support with 7.5 % Nafion.

A spraying method was used to prepare MEAs. At low potentials (1.45 and 1.65V) 1.0mgIr/cm^2 loaded MEA showed the highest performance and the trend of the current at certain potential vs. loading was fairly linear since the reaction is kinetic control thus increase in loading means increase in active surface area so more active site for the reaction to happen. At high potentials (1.85V) 0.8mgIr/cm^2 showed the highest performance with 2.1A/cm^2, since the kinetics is not the only factor and mass transport, proton and electron conductivity are of importance. In addition significant increase in performance was obtained by coating titanium backing plates by gold which is thought to occur due to increase in contact points and decrease in contact resistance.

In order to enlighten the reaction distribution and discover an ideal layer thickness, a theoretical model developed for current and reaction rate distribution through the porous layer based on Tafel polarization in terms of layer thickness, total current, proton, and electron conductivity. Theoretical analysis supported experimental data at low potentials and its deviation at high potentials was discussed and corrected by adding a factor according to reduction of active surface area by decrease in layer thickness.

Cross-sections of the MEAs were studied using SEM and TEM. Catalyst layer thickness was found to be in the range of 2 to 5µm for loadings from 0.4 to 1.0mgIr/cm^2. Accelerated degradation test protocol introduced, and test results were corrected subtracting ohmic resistance due to degradation and corrosion of current collectors and other resistances. The loss found to be 0.3mV/h during the degradation test. Comparison of TEM images of the cross-section before and after degradation test showed transport of Iridium particles from the active layer into the membrane which+ thought to be the major cause of performance loss.

6 Future work

Although some aspects of MEA preparation were studied and a model was proposed for current distribution through the catalyst layer, still many features and conditions remain unclear. Suggested future work could be:

- Adding a conductive layer on the top of the oxygen electrode to increase the connection points between catalyst layer and current collector to enhance catalyst utilization
- Taking the model to two or three dimensions for better understanding of the reaction rate and current distribution through the catalyst layer
- Developing the model in order to relate catalyst and Nafion conductivity to utilization of the MEA
- Studying the water purity during water electrolysis and its effect on the performance
- Utilize the Nafion content in catalyst layer and loading at the same time using factorial design.
- Scaling up the area of the catalyst layer using automated spraying apparatus

7 References

1. C. J. Winter. Hytime-it's high time for hydrogen energy business forum. *Int. J. Hydrogen Energy*. 22 (9): 847-857, 1997
2. D. G. Kessel. Global warming-facts, assessment, countermeasures. *J.Petroleum Sci. and Engeneering*. 26: 157-168, 2000
3. A. Marshall. *Electrocatalysts for the Oxygen ecolution in water electrolyzers using PEM.* Ph.D. thesis, NTNU, Trondheim, Norway, 2005
4. H. Takenaka, E. Torikai, Y. Kawami, N. Wakabayashi. Solid polymer electrolyte water electrolysis. *Int. J. Hydrogen Energy*, 7: 397,1989.
5. P. Millet, M. Pineri, R. Durand, New solid polymer electrolyte composites for water electrolysis *J. Appl. Electrochem.*, 19: 162,1989.
6. F. Andolfatto, R. Durand, A. Michas, P. Millet, P. Stevens, Solid Polymer Electrolyte water electrolysis : electrocatalysis and long term stability.*Int. J. Hydrogen Energy*, 19 :421, 1994.
7. E. Slavcheva, I. Radev, S. Bliznakov, G. Topalov, P. Andreev, E. Budevski**.** Sputtered iridium oxide films as electrocatalysts for water splitting via PEM electrolysis. *Electrochem. Acta,* 52: 3889, 2007.
8. E. Rasten. *Electrocatalysis in Water Electrolysis with Solid Polymer.* Ph.D. thesis, NTNU, Trondheim, Norway, 2001
9. Zhang, Juijun**.** *PEM fuel cell electrocatalysts and catalysts layer.* London : Speringer Verlag, 2008.
10. Y. Nishimura, K. Yasuda, Z. Siroma, and K. Asaka. High current density solid polymer electrolyte water electrolysis. *Denki kagaku oyobi kogyo butsuri kagaku,* 65: 1122-1123, 1997
11. R.D. Mussel, T.J. Regh, Active Layer for Membrane Electrode Assembly. The Dow Chemical Company, *US Patent 5*,882,810 (1999).
12. H. Wendt**.** *Electrochemical hydrogen technologies.* New York : Elsevier, 1990. pp. 3-4.
13. H. Hamann, A. Hamnett, W. Vielstich. *Electrochemistry.* Weinhem : Wiley, 2007. pp. 159-168.
14. Trasatti, Sergio. Interfacial electrochemisty of conductive oxides for electrocatalysis: J *appl electrochem*,23:769-788, 1995
15. Trasatti, S. Work function, electronegativity, and electrochemical behaviour of metals. *J. Electroanal. Chem*, 39: 163-169,1979
16. Ji-M, J-Q. Z., Chu-Nan C.Oxygen revolution reaction on IrO2-based DSA type electrodes: kinetics analysis of Tafel lines and EIS. *International Association for electrochemistry.*49:791-797,2004
17. Boodts, JFC, Fergonara, G and Trasatti, S. Performance of electrodes for industrial electrochemical processes. *The electro chemical society*, 136: 135-140, 1995

18. Chen, Linlin, Guay, Daniel and Pollak. AFM observation of surface activation of ruthenium oxide electrodes during hydrogen evolution. *J electroanal chem*,429: 185-192, 1997.
19. Hamment, A, Stevens, PS and wingate. Nafion bonded porous titanium oxide electrodes for oxygen evolution: towards a regenerative fuel cell. J*ournal of electrochemistry*, 21: 982-985, 1991
20. S. Trasatti. Electrocatalysis in the anodic evolution of oxygen and chlorine. *Electrochim. Acta*, 29:1503–1512, 1984.
21. Barbaro, P and Bianchini, C. *Catalysis for Sustainable Energy Production.* England : Wiley, 2009.
22. J larminie, A Dicks. *Fuel Cell systems explained.* England : Wiley, 2003
23. H. Tawfik, Y. Hung, D. Mahajan. Metal bipolar plates for PEM fuel cell-A review *Journal of Power Sources*, 163 : 755–767, 2007
24. Sulentic, Ines. *Synthesis and characterization of electrocatalyst for oxygen evolution reaction in PEMWE.* Tronheim : Bachelor Thesis, Trondheim, Norway 2010.
25. Yoshida, N. T. Ishisaki, A. Watakabe . M. Yoshitake**.** Characterization of Flemion® membranes for PEFC. *Elsevier Ltd.* 43*:* 3749-3754, 1998
26. C. Boyer, S. Gamburzev, O. Velev, S. Srinivasan, A.J. Appleby. Measurments of proton conductivity in the active layer of PEM fuel cell gas diffusion electrodes. *Electrochemical acta.*43: 3703-3709, 1998
27. Shao, Yuyan, Novel catalyst support materials for PEM fuel cells, *Journal of Materials Chemistry,* 19: 46-59, 2008
28. A. H. Zavieh. In-situ Characterization and optimization of electrocatalysts for oxygen evolution in water electrolysis using proton exchange membranes, Master Project, NTNU, Trondheim, 2010
29. J. Newman. K. E. Thomas. *Electrochemical systems-third edition.* John Wiley, Hoboken, Newjersy, 2004
30. Qiangu Yan, Junxiao Wub. Modeling of single catalyst particle in cathode of PEM fuel cells. *Energy Conversion and Managemen*t. 49: 2425–2433, 2008
31. Kinoshita K. Small-particle effects and structural considerations for electrocatalysis. *Modern Aspects of Electrochemistry*,14: 557–637,1982
32. Mukerjee S. Particle size and structural effects in platinum electrocatalysis. *J Appl Electrochem* 20:537-542, 1990
33. J. S. Newman, C. W. Tobias. Theoretical analysis of current distribution in porous electrodes. *J of electrochemical Society*. 109: 1183-1191, 1962
34. D. Williams, C. Carter. *Transmission Electron Microscopy.* s.l. : Plenum Press, 1996.
35. K. Dretvik, *Supported Ir catalyst of oxygen evolution,* Master Thesis, NTNU, Trondheim, 2011
36. H. A. Gasteiger , J. E. Panels S. G. Yan. Dependence of PEM fuel cell performance on catalyst Loading. *Journal of Power Sources* 127: 162-171, 2004

37. Trassati, Electrocatalysis in the anodic evolution of oxygen and chlorine. *Electrochimica acta*, 29: 1503-1512, 1984
38. Yuyan Shao, Geping Yin, Yunzhi Gaoa. Understanding and approaches for the durability issues of Pt-based catalysts for PEM fuel cell. *Journal of Power Sources.* 171: 558-566, 2007
39. P. Millet, R. Ngameni, S.A. Grigoriev, N. Mbemba, F. Brisset, A. Ranjbari,C. Etiévant. PEM water electrolyzers: From electrocatalysis to stack development. International *Journal of Hydrogen Energy*. 35: 5043-5052,2010
40. Shidong Song, Huamin Zhang, Xiaoping Ma, Zhigang Shao, Richard T. Baker, Baolian Yi. Electrochemical investigation of electrocatalysts for the oxygen evolution reaction in PEM water electrolyzers. *International journal of hydrogen energy*. 33: 4955-4961, 2008

Appendix A

7.1 A.1 Density and porosity of the catalyst layer

$$\rho = \frac{m}{V}$$

Ir density: 22.56 g/cm^3, ATO density: 6.8 g/cm^3, Nafion density: 1.98 g/cm^3

Theoretical Catalyst density (20%Ir/ATO): 7.93 g/cm^3

Theoretical Catalyst Layer density (Ir/ATO/Nafion7.5%): 6.49 g/cm^3

Real Catalyst layer thickness: 4.6 µm

Real Catalyst layer mass: 0.8 mg/cm^2

Real catalyst layer density: 1.73 g/cm^3

$$porosity = 1 - \frac{real\ density}{theoretical\ density}$$

Porosity percentage of the layer is 73%

7.2 A.2 Catalyst conductivity

The catalyst conductivity was measured using apparatus shown in figure 6-1, 500 mg of the catalyst was put in the cylinder and the height was measured precisely then the resistance was determined from the slope of the curve potential versus current scanning the potential from 0.00V to 0.500V vs. SHE with a scan rate of 1.00mV s^{-1}.

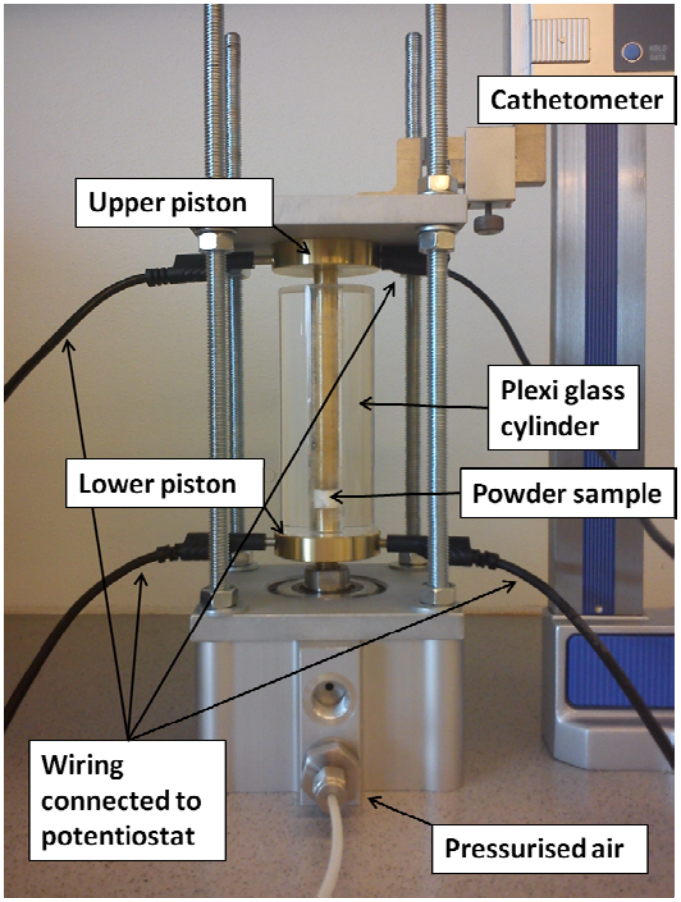

Figure A-1 apparatus used to measure powder conductivity [35]